

Beyond Procedure: Substantive Fairness in Conformal Prediction

Pengqi Liu ^{*1} Zijun Yu ^{*1} Mouloud Belbahri ² Arthur Charpentier ³ Masoud Asgharian ¹ Jesse C. Cresswell ⁴

Abstract

Conformal prediction (CP) offers distribution-free uncertainty quantification for machine learning models, yet its interplay with fairness in downstream decision-making remains underexplored. Moving beyond CP as a standalone operation (*procedural* fairness), we analyze the holistic decision-making pipeline to evaluate *substantive* fairness—the equity of downstream outcomes. Theoretically, we derive an upper bound that decomposes prediction-set size disparity into interpretable components, clarifying how label-clustered CP helps control method-driven contributions to unfairness. To facilitate scalable empirical analysis, we introduce an LLM-in-the-loop evaluator that approximates human assessment of substantive fairness across diverse modalities. Our experiments reveal that label-clustered CP variants consistently deliver superior substantive fairness. Finally, we empirically show that equalized set sizes, rather than coverage, strongly correlate with improved substantive fairness, enabling practitioners to design more fair CP systems. Our code is available at <https://github.com/layer6ai-labs/llm-in-the-loop-conformal-fairness>.

1. Introduction

Conformal prediction (CP) (Vovk et al., 2005; Shafer & Vovk, 2008) provides finite-sample, distribution-free statistical guarantees through a well-defined procedure; yet, whether these *procedural* guarantees translate into *equitable outcomes* in downstream decision-making remains unclear. In high-stakes domains, reliable uncertainty quantification is essential for building trustworthy models. Unlike other methods that rely on strong assumptions about the data distribution (Gal & Ghahramani, 2016; Lakshminarayanan

^{*}Equal contribution, alphabetical order. ¹McGill University, Montreal, Canada ²TD Insurance, Montreal, Canada ³UQAM, Montreal, Canada ⁴Layer 6 AI, Toronto, Canada. Correspondence to: Pengqi Liu <pengqi.liu@mail.mcgill.ca>.

Preprint. February 20, 2026.

et al., 2017) or require architectural modifications (Neal, 2012), CP is distribution-free, model-agnostic, and applies directly to any black-box predictor (Angelopoulos & Bates, 2021). However, the rigorous procedural nature of CP does not automatically ensure equitable outcomes, necessitating a deeper investigation into how these statistical bounds influence fairness in practice.

Fairness in machine learning (Barocas et al., 2023), particularly in regulated fields such as healthcare and finance, is commonly understood through two complementary perspectives: *procedural fairness*, which concerns the integrity of the decision process (e.g., fairness through unawareness (Zemel et al., 2013; Kusner et al., 2017)); and *substantive fairness*, which focuses on equitable outcomes across groups (e.g., Equalized Odds (Hardt et al., 2016)). Prior research in CP has mainly focused on procedural fairness, treating CP as a standalone process (Romano et al., 2020a). In practice, CP constitutes one step in a larger pipeline that includes downstream decisions. The interactions of CP with procedural and substantive notions of fairness in this broader context remain less well understood (Cresswell, 2025).

In this work, we move beyond viewing CP as a standalone operation to analyze the *holistic* decision-making pipeline. While ultimate fairness is defined by substantive outcomes, procedural choices within CP play a critical role in shaping these results. We aim to uncover the specific connections between procedural properties and substantive fairness, enabling the design of procedures that positively influence downstream equity. By evaluating fairness as an emergent property of the entire pipeline, we can distinguish between procedural metrics that are merely performative and those that genuinely drive fair outcomes.

Our main contributions are threefold:

Scalable LLM-in-the-loop fairness evaluation. To overcome the resource constraints of human-subject experiments, we leverage large language models (LLMs) in an evaluation protocol that approximates human decision behavior. We validate that this evaluator produces results comparable to human-in-the-loop benchmarks, enabling us to scale our analysis of substantive fairness across a broader range of datasets and algorithms than prior work.

Connecting procedural properties to substantive fairness. We explicitly map the relationships between procedu-

ral CP metrics and substantive outcomes. Crucially, we find that *Equalized Set Size* correlates strongly with improved substantive fairness, whereas the standard goal of *Equalized Coverage* often has negative effects. This insight shifts the design objective from coverage parity to set size parity.

Theoretical and empirical validation of Label-Clustered CP. Guided by the connection between set sizes and substantive fairness, we analyze Label-Clustered CP. We derive a theoretical upper bound decomposing the set size disparity into interpretable components. Experimentally, we confirm that Label-Clustered CP reduces set size disparity more effectively than marginal or group-conditional approaches, and consistently achieves the best substantive fairness results in our evaluations.

2. Background

2.1. Conformal Set Predictors

Consider inputs $x \in \mathcal{X} \subset \mathbb{R}^d$ with ground truth labels $y \in \mathcal{Y} = [m] := \{1, \dots, m\}$, drawn from a joint distribution $(x, y) \sim \mathbb{P}$. Let $f : \mathcal{X} \rightarrow \Delta^{m-1} \subset \mathbb{R}^m$ be a classifier outputting predicted probabilities, where Δ^{m-1} is the $(m-1)$ -dimensional probability simplex. CP constructs a set-valued function $\mathcal{C} : \mathcal{X} \rightarrow \mathcal{P}(\mathcal{Y})$ where $\mathcal{P}(\mathcal{Y})$ denotes the power set of \mathcal{Y} , such that the following marginal coverage guarantee holds,

$$\mathbb{P}[y \in \mathcal{C}(x)] \geq 1 - \alpha, \quad (1)$$

where $\alpha \in [0, 1]$ is user-specified (Vovk et al., 1999; 2005).

CP achieves coverage by varying set size $|\mathcal{C}(x)|$ based on a calibrated notion of model confidence. Calibration relies on a held-out dataset $\mathcal{D}_{\text{cal}} = \{(x_i, y_i)\}_{i=0}^{n_{\text{cal}}}$ consisting of n_{cal} datapoints drawn from \mathbb{P} . A *conformal score function* $s : \mathcal{X} \times \mathcal{Y} \rightarrow \mathbb{R}$ measures non-conformity between a candidate label and an input datapoint x , with higher scores indicating poorer agreement. The score function is often defined to make use of information from the classifier f in judging the level of agreement.

Let $S_i := s(x_i, y_i)$ for $i \in [n_{\text{cal}}]$, and define

$$\tau_\alpha := \frac{[(n_{\text{cal}} + 1)(1 - \alpha)]}{n_{\text{cal}}} \in (0, 1]. \quad (2)$$

The empirical conformal threshold is then given by

$$\hat{q}_\alpha := \text{Quantile}_{\tau_\alpha}(S_1, \dots, S_{n_{\text{cal}}}) \in \mathbb{R}. \quad (3)$$

For a test point x_{test} drawn from the x -marginal of distribution \mathbb{P} , a *conformal prediction set* is constructed as

$$\mathcal{C}_{\hat{q}_\alpha}(x_{\text{test}}) := \{y \in \mathcal{Y} \mid s(x_{\text{test}}, y) \leq \hat{q}_\alpha\}. \quad (4)$$

Sets constructed this way will satisfy $1 - \alpha$ coverage (Equation (1)) for any score function s , but smaller sets are more

useful for downstream uncertainty quantification applications (Cresswell et al., 2024). The average set size $\mathbb{E}[|\mathcal{C}|]$ is dictated by the quality of s , and in turn by the accuracy and calibration of the classifier f . Efficient score functions like APS (Romano et al., 2020b), RAPS (Angelopoulos et al., 2021), and SAPS (Huang et al., 2024) aim to minimize $\mathbb{E}[|\mathcal{C}|]$ while maintaining coverage.

2.2. Fairness Notions for Set Predictors

We briefly review common fairness notions in machine learning and discuss how they apply to conformal set predictors. Let $\mathcal{A} = [k_g]$ denote a finite set of sensitive group labels, and let $g : \mathcal{X} \rightarrow \mathcal{A}$ be a group assignment function. Each group is defined as

$$G_a := \{x \in \mathcal{X} : g(x) = a\}, \quad a \in \mathcal{A}. \quad (5)$$

Fairness via non-discrimination criteria. In classical supervised learning with point predictions, statistical fairness notions often require parity of prediction behavior across groups. For example, demographic parity requires

$$\mathbb{P}(\hat{y} = 1 \mid X \in G_a) = \mathbb{P}(\hat{y} = 1 \mid X \in G_b), \quad \forall a, b \in \mathcal{A},$$

with $y = 1$ denoting some important outcome, while Equalized Odds further conditions on the true label (Hardt et al., 2016). These criteria aim to ensure that outcomes are not systematically skewed by group membership, and hence are aligned with substantive fairness—the predominant paradigm for fairness in regulatory frameworks (OCC, 2026), and in machine learning (Green, 2022).

In CP, non-discrimination fairness is commonly formulated in terms of *group-conditional coverage*, where \mathcal{C} satisfies

$$\mathbb{P}[y \in \mathcal{C}(x) \mid x \in G_a] \geq 1 - \alpha, \quad \forall a \in \mathcal{A}. \quad (6)$$

Each group receives the same nominal statistical guarantee, achieving *Equalized Coverage* (Romano et al., 2020a). **Mondrian CP** achieves Equation (6) by using the predefined grouping function g to calibrate conformal thresholds separately within each group (Vovk et al., 2003). Since this means partitioning the calibration set \mathcal{D}_{cal} , each group is calibrated on a smaller sample, leading to increased variance of empirical coverage (Zwart, 2025; Gibbs et al., 2025).

However, Equalized Coverage focuses on the construction of prediction sets—an intermediate tool for uncertainty quantification. Hence it is a procedural notion, ignoring how sets are used and what their downstream impact may be. Cresswell et al. (2025) showed via randomized controlled trials that equalizing coverage causes disparate impact in downstream tasks where people use prediction sets as decision aids. *Equalized Set Size* was proposed as an alternative fairness notion for CP. While still procedural in nature, this notion better correlated with reduced disparate impact.

2.3. Advanced Conformal Prediction Variants

Beyond marginal and group-conditional coverage, several CP variants target alternative statistical guarantees. Exact conditional coverage at every $x \in \mathcal{X}$ is known to be impossible without strong assumptions (Vovk, 2012; Lei et al., 2013; Foygel Barber et al., 2021). Instead, clustered conformal prediction (Ding et al., 2023) seeks approximate conditional coverage by partitioning the *label space* into clusters via a learned clustering function $h : \mathcal{Y} \rightarrow [K]$, and calibrating independent thresholds \hat{q}_k for each cluster $k \in [K]$. For a test input x_{test} , each label y is included in $\mathcal{C}(x_{\text{test}})$ if its score $s(x_{\text{test}}, y)$ is below the threshold $\hat{q}_{h(y)}$. Clustered conditional coverage follows as

$$\mathbb{P}[y_{\text{test}} \in \mathcal{C}(x_{\text{test}}) \mid h(y_{\text{test}}) = k] \geq 1 - \alpha, \quad (7)$$

for all clusters. This adapts thresholds to label-specific difficulty, yielding empirically improved conditional coverage without requiring predefined instance groups.

The same partitioning-through-clustering strategy also applies when we partition the *group space* into clusters via a learned clustering function $\tilde{h} : \mathcal{A} \rightarrow [K]$, and calibrate independent thresholds for each cluster of groups. We refer to these two methods as **Label-Clustered** and **Group-Clustered** CP, respectively.

Backward CP (Gauthier et al., 2025) reverses the usual prioritization: instead of fixing the coverage level α and accepting variable set sizes, it constrains the set size via a data-dependent rule \mathcal{T} while providing a relaxed marginal coverage guarantee:

$$\mathbb{P}[y_{\text{test}} \in \mathcal{C}(x_{\text{test}})] \geq 1 - \mathbb{E}[\tilde{\alpha}], \quad (8)$$

where the random variable $\tilde{\alpha} > 0$ is chosen to respect the size constraint. The prediction set is constructed using *e-values* (Vovk, 2025) derived from the non-conformity scores; labels with sufficiently small e-values are included until the size constraint is reached.

Detailed mathematical formulations and pseudocode for Marginal, Mondrian, Label-Clustered, Group-Clustered, and Backward CP are provided in Appendix B.

3. Related Work

The study of fairness in applications of CP is an emergent field, and several alternative directions have recently been introduced. Initially researchers adopted Equalized Coverage (Romano et al., 2020a; Zhou & Sesia, 2024) and suggested pursuing it in deployments of CP (Lu et al., 2022; Zerva & Martins, 2024; Garcia-Galindo et al., 2025). More recently this standard has been reexamined, with significant concerns being raised about its practical consequences (Cresswell et al., 2025). More broadly, researchers have applied existing group algorithmic fairness notions to prediction sets,

including demographic parity (Liu et al., 2022), Equal Opportunity (Wang et al., 2024), and others (Vadlamani et al., 2025). Individual fairness notions like counterfactual fairness (Kusner et al., 2017) have also been extended to CP (Guldogan et al., 2025).

While these notions have been applied in various settings (Kuchibhotla & Berk, 2023; Berk et al., 2023; Srinivasan et al., 2025), the fairness definitions above pertain only to coverage and the construction of prediction sets, rather than impact in downstream tasks. One exception is the work of Tasar (2025), which defers decisions to an alternate process—such as a human-in-the-loop—unless the model expresses confidence via a singleton prediction set. They propose the *deferral gap*—the difference in deferral rates across groups—as a substantive fairness metric. However, they only instantiated the alternate process through random class assignment which decouples the assessment of fairness and prediction set properties from downstream task performance. In contrast, we incorporate downstream usage directly into our definition and measurement of fairness.

4. Methodology

Group-conditional coverage (Equation (6)) is a natural *procedural* fairness goal for CP, but coverage alone does not fully characterize fairness in downstream decision-making. In particular, prediction sets with equal coverage may differ systematically across groups in size or informativeness, leading to unequal benefits when these sets are used by humans or automated decision rules (Cresswell et al., 2025). Our ultimate goal is to promote substantive fairness in downstream decision-making by using prediction sets. To this end, we develop a robust evaluation framework for assessing substantive fairness of CP methods. Using this pipeline, we study how procedural fairness notions (e.g., Equalized Coverage and Equalized Set Size) affect substantive fairness, how substantive fairness changes with different prediction-set characteristics, and which CP methods are most effective for supporting equitable downstream performance.

As noted by Cresswell et al. (2025), equalizing coverage can increase set size disparities, which may in turn amplify substantive unfairness. Motivated by this finding, we focus our analytical work on approaches that prioritize equalizing set size rather than equalizing coverage. Concretely, we consider Label-Clustered CP, discussed in Section 2.3, which mitigates set size disparity by clustering similar datapoints regardless of group. In this section we theoretically justify why Label-Clustered CP reduces set size gaps, then present our evaluation framework for assessing substantive fairness in CP.

4.1. Label-Clustered CP Reduces Set Size Disparity

Let $A \in \mathcal{A}$ be the protected attribute and consider groups $a, b \in \mathcal{A}$. The expected set size disparity between groups is

$$\Delta_{a,b} = |\mathbb{E}[|\mathcal{C}(X)| \mid A=a] - \mathbb{E}[|\mathcal{C}(X)| \mid A=b]|. \quad (9)$$

For Label-Clustered CP we derive an upper bound that decomposes $\Delta_{a,b}$ into three interpretable components which can explain why label clustering often empirically yields smaller $\Delta_{a,b}$ than Marginal or Mondrian CP. This bound makes explicit how the number of clusters K affects method-driven components in $\Delta_{a,b}$.

Theorem 4.1 (Label-Clustered CP set size disparity bound).

Fix any label-clustering map $h : \mathcal{Y} \rightarrow [K]$ and let $\mathcal{Y}_k := \{y \in \mathcal{Y} : h(y) = k\}$. Consider a label-clustered conformal set predictor \mathcal{C} that uses cluster-specific thresholds. For any $y \in \mathcal{Y}$, $k \in [K]$, and group $a \in \mathcal{A}$, define

$$\mu_{k,a} := \mathbb{E}[|\mathcal{C}(X)| \mid h(Y) = k, A = a], \quad (10)$$

$$r_{y,a} := \mathbb{E}[|\mathcal{C}(X)| \mid Y = y, A = a], \quad \text{and} \quad (11)$$

$$\epsilon_{k,a} := \max_{y \in \mathcal{Y}_k} r_{y,a} - \min_{y \in \mathcal{Y}_k} r_{y,a}. \quad (12)$$

Then, for any two groups a, b ,

$$\begin{aligned} \Delta_{a,b} \leq & \underbrace{\max_{k=1,\dots,K} \epsilon_{k,a}}_{(I): \text{Intra-cluster label heterogeneity}} + \underbrace{\left(\max_{k=1,\dots,K} \mu_{k,a} - \min_{k=1,\dots,K} \mu_{k,a} \right)}_{(II): \text{Cross-cluster spread}} \\ & + \underbrace{\left| \sum_{y \in \mathcal{Y}} \mathbb{P}(Y = y \mid A = b) (r_{y,a} - r_{y,b}) \right|}_{(III): \text{Intra-label cross-group disparity}}. \end{aligned} \quad (13)$$

The proof of Theorem 4.1 is given in Appendix A, with a detailed justification of why Label-Clustered CP reduces set size disparity across groups. Here, we provide interpretations and implications of Theorem 4.1. The quantities we define each break down labels, groups, and clusters in different ways: $\mu_{k,a}$ represents the expected set size of a given group in a given cluster (across labels), while $r_{y,a}$ looks at label y within group a (across clusters). $\epsilon_{k,a}$ is the spread of set size across labels in cluster k , conditioned on one group.

Theorem 4.1 highlights three drivers of set size disparity:

(I) **Intra-cluster label heterogeneity**: If clusters bring together labels with similar difficulty levels, then labels within each cluster tend to have similar expected set sizes, making each $\epsilon_{k,a}$ small. This explains why $K = 1$ (Marginal CP) can yield a large $\epsilon_{1,a}$ – all labels are forced into a single cluster, so intra-cluster label heterogeneity can be high.

(II) **Cross-cluster spread**: Consider the case of $K = |\mathcal{Y}|$ where each label forms a cluster. Although the intra-cluster label heterogeneity is minimized ($\epsilon_{k,a} = 0$), conformal thresholds become unstable for rare labels, yielding large disparity in set size between clusters. With a proper choice of K , Label-Clustered CP can make the expected set size

more comparable across clusters while controlling $\epsilon_{k,a}$.

(III) **Intra-label cross-group disparity** captures set size disparity between groups but within labels. Compared to Mondrian CP, Label-Clustered CP avoids inflating this component because it uses shared thresholds across protected groups (within each label-cluster) and pools calibration data across groups, reducing variance and preventing artificial group differences; see Appendix A for detailed comparison.

Overall, the bound in Equation (13) highlights two clustering-dependent drivers: intra-cluster label heterogeneity and cross-cluster spread. In our experiments we study the behaviour of these terms individually.

4.2. LLM-in-the-loop Substantive Fairness Evaluation

Evaluating the downstream impact of CP on decision-making typically requires expensive and difficult-to-scale human trials. To address this, we propose an **LLM-in-the-loop** evaluation framework which offers key advantages: (i) LLMs exhibit approximate i.i.d. behavior across evaluations, avoiding human fatigue, learning effects, and temporal drift which all increase variance; (ii) they are adaptable to heterogeneous tasks across diverse data modalities; (iii) they allow for scalable, robust statistical evaluation. Most importantly, we show that our LLM-in-the-loop evaluator reproduces the same qualitative ordering of substantive fairness metrics observed in prior human-in-the-loop experiments (Cresswell et al., 2025)—particularly that Mondrian CP exhibits higher disparate impact than Marginal (see Section 6.1 and Appendix E.1). In this section, we define substantive fairness within this framework and detail our estimation procedure using Generalized Estimating Equations (GEE).

Substantive fairness as decision improvement. We ground our definition of substantive fairness in the concrete benefit provided to the decision-maker. Let $\text{Acc}(x, \hat{y}, \mathcal{C}(x))$ denote the decision accuracy achieved by the agent that predicts \hat{y} given input x and prediction set $\mathcal{C}(x)$. We define the *group-specific improvement* as the expected lift in utility provided by the CP method relative to a control baseline where the agent acts without a prediction set (i.e., $\mathcal{C}(x) = \emptyset$). For a protected group $a \in \mathcal{A}$, this is given by

$$\delta_{t,a} := \mathbb{E}[\text{Acc}(x, y, \mathcal{C}_t(x)) - \text{Acc}(x, y, \emptyset) \mid x \in G_a],$$

where t stands for a CP method. For substantive fairness we require that the improvement be consistent across groups, i.e., there is no disparate impact. Hence, we quantify unfairness as the maximum disparity between groups:

$$\Delta_t := \max_{a,b \in \mathcal{A}} |\delta_{t,a} - \delta_{t,b}|. \quad (14)$$

A disparity $\Delta_t \approx 0$ indicates that the CP method t improves downstream decision-making equally for all groups.

Estimation of Δ_t via Generalized Estimating Equations. Directly computing empirical averages for Equation (14)

is prone to confounding factors, such as systematic variations in task difficulty and the agent’s willingness to rely on the provided sets. To obtain robust, statistically valid estimates of Δ_t , and to take into account the correlation among predictions made for the same task under the assistance of different CP sets, we employ a logistic GEE regression.

For any data modality we assume access to a predictive model used to generate conformal sets via a CP algorithm t and fixed score function. We then provide an LLM (or multimodal foundation model) with a description of the task, a test datapoint x_j , corresponding prediction set $\mathcal{C}_t(x_j)$, and a statement of the coverage guarantee (i.e., $1 - \alpha$). The LLM is used to generate M independent predictions \hat{y}_{jt}^m , $m \in [M]$. Then we define $R_{jt} := \frac{1}{M} \sum_{m=1}^M \mathbf{1}\{\hat{y}_{jt}^m = y_j\}$, the proportion of correctly predicted responses for x_j with CP method t . We model the probability of correctness with key covariates and clustering by task to account for intra-instance correlations, for which GEEs are suitable (Liang & Zeger, 1986). The regression model is specified as

$$\text{logit}(\mathbb{E}[R_{jt}]) \sim \text{treat}_t \times \text{group}_j + \text{diff}_j + \text{adoption}_{jt}. \quad (15)$$

Here, group_j is the group that x_j belongs to, $\text{treat}_t \times \text{group}_j$ captures the interaction of interest; diff_j approximates task difficulty (using Marginal CP set size); and adoption_{jt} measures the proportion of the agent’s predictions adopted from the provided set $\mathcal{C}_t(x_j)$. This adoption covariate is crucial for generalizing results, as it accounts for varying levels of faith the agent places in the CP sets it is shown.

Quantifying fairness with maxROR . From the fitted GEE model, we compute the marginal probability $p_{t,a}$ of a correct response for treatment t and group a . We convert these probabilities into odds ratios (ORs) relative to the control baseline:

$$\text{OR}_{t,a} := \frac{p_{t,a}/(1 - p_{t,a})}{p_{\text{control},a}/(1 - p_{\text{control},a})}. \quad (16)$$

$\text{OR}_{t,a} > 1$ indicates that treatment t improves the LLM’s accuracy for group a , compared to the control. To measure the disparity of improvement across groups a and b , we compute the ratio of odds ratios (ROR) and take the maximum over all pairs. This yields our primary metric for substantive fairness, the **maxROR**:

$$\text{maxROR}_t := \max_{a,b \in \mathcal{A}} \left(\frac{\text{OR}_{t,a}}{\text{OR}_{t,b}} \right) - 1. \quad (17)$$

maxROR is a principled way of measuring disparity (Equation (14)) that accounts for factors such as the difference in difficulty between groups. A maxROR_t close to zero implies no downstream disparate impact from the use of CP method t , while a value of 0.10 (10%), for example, indicates that one group benefited 10% more than another. We primarily report **maxROR %** values from our LLM-in-the-loop evaluator to quantify substantive fairness. Additional technical details on the evaluator are given in Appendix C.

5. Experimental Setup

5.1. Experimental Design

Our experiments investigate the interplay of procedural and substantive fairness notions in CP. We employ the LLM-in-the-loop evaluator described in Section 4.2 to answer four core research questions:

RQ1 Alignment: *Does the LLM-in-the-loop evaluator faithfully reflect decision-making behaviors observed in humans?* We validate that our LLM-in-the-loop evaluator aligns with prior human-subject studies, showing that it is a meaningful proxy, enabling scalable substantive fairness evaluation.

RQ2 Substantive Benchmarking: *Which CP methods achieve substantive fairness, while still being useful?* We evaluate several CP methods to determine which is most fair in downstream tasks (lowest **maxROR**), with overall utility of the prediction sets in mind.

RQ3 Metric Correlation: *Do procedural fairness metrics correlate with substantive fairness?*

We analyze the relationship between procedural notions (Equalized Coverage, Equalized Set Size) and our substantive metric (**maxROR**) to determine if procedural metrics can be diagnostic indicators of downstream fairness.

RQ4 Theoretical Verification: *Can our theoretical analysis of Label-Clustered CP be experimentally verified?*

We validate our theoretical analysis of set size disparity for Label-Clustered CP (Section 4.1) through ablations and numerical studies.

Further details on datasets, CP score functions, hyperparameter tuning, and prompt engineering for the LLM-in-the-loop are provided in Appendix D. Our code implementing CP methods and the LLM evaluator on these tasks is available at this [Github repo](#).

5.2. Tasks, Datasets, and Models

We evaluate our methods on four prediction tasks spanning vision, text, audio, and tabular modalities, using open-access datasets commonly studied in algorithmic fairness. In all settings, CP is applied to the outputs of task-specific base models to construct prediction sets, and a foundation model uses those sets as decision aids on the downstream task.

Image Classification. We use the FACET dataset (Gustafson et al., 2023), predicting one of 20 occupation classes from images. Age (Younger, Middle, Older, Unknown) defines the protected groups. Prediction sets are generated using a zero-shot CLIP ViT-L/14 model as the base model (Dosovitskiy et al., 2021; Radford et al., 2021), while Qwen2.5-VL-7B-Instruct is used as the LLM-in-the-loop for its vision-language capabilities (Bai et al., 2025).

Text Classification. We consider occupation prediction on

Table 1. Base Model and CP Method Metrics on $\mathcal{D}_{\text{test}}$.

Task	Acc	Δ_{Acc}	CP Method	Cvg	Size
FACET	70.0	22.2	Marginal	89.9	2.62
			Mondrian	89.9	2.66
			Label-Clustered	89.1	2.92
			Group-Clustered	89.3	2.51
			Backward	90.1	3.50
BiosBias	78.9	2.70	Marginal	89.5	1.68
			Mondrian	90.0	1.80
			Label-Clustered	90.3	1.75
			Group-Clustered	90.2	1.75
			Backward	91.5	2.50
RAVDESS	70.3	6.11	Marginal	88.3	1.89
			Mondrian	87.5	1.86
			Label-Clustered	87.8	1.92
			Group-Clustered	87.5	1.90
			Backward	91.9	2.48
ACSincome	31.0	5.71	Marginal	89.8	5.35
			Mondrian	89.5	7.16
			Label-Clustered	89.9	5.33
			Group-Clustered	89.8	5.37
			Backward	92.3	6.50

Table 2. Human vs. LLM Evaluator Comparison (maxROR %).

Dataset	Human-in-the-loop		LLM-in-the-loop	
	Marginal	Mondrian	Marginal	Mondrian
FACET	26	51	9.0	38
BiosBias	12	33	6.9	8.1
RAVDESS	1.0	28	11	79

the BiosBias dataset (De-Arteaga et al., 2019), restricted to the 10 most frequent classes with binary gender as the sensitive attribute. A linear classifier trained on frozen BERT representations (Devlin et al., 2019) acts as the base model, and GPT-4o-mini as the LLM-in-the-loop (OpenAI, 2024).

Audio Emotion Recognition. We use the RAVDESS dataset (Livingstone & Russo, 2018) to classify audio clips into eight emotion classes, with binary gender as the group attribute. Base predictions are obtained from a fine-tuned wav2vec 2.0 model (Baevski et al., 2020), and GPT-4o-audio-preview acts as the LLM-in-the-loop for its audio capabilities (OpenAI, 2026).

Tabular Prediction. We predict income brackets on the ACSIncome dataset from Folktables (Ding et al., 2021), using race (aggregated) as the group attribute. An XGBoost classifier (Chen & Guestrin, 2016) is the base model, while Qwen2.5-7B is the LLM-in-the-loop (Yang et al., 2024a).

Table 1 shows a summary of base model and CP metrics on the test set, including accuracy and the maximum accuracy gap between groups, Δ_{Acc} . Cvg is the empirical coverage, and Size is the average set size, where $1 - \alpha = 0.9$. Metrics are not averaged across calibration-test splits.

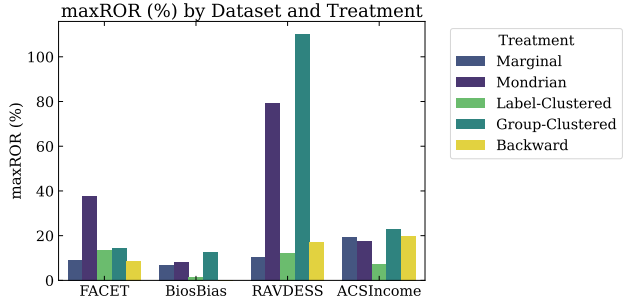


Figure 1. maxROR (%) of each CP method across four tasks. Lower is more substantively fair.

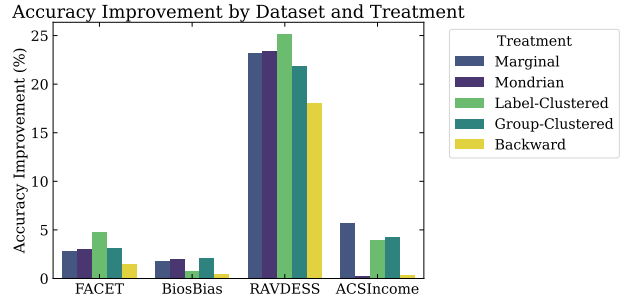


Figure 2. Accuracy improvement (%) relative to Control of each CP method, across four tasks. Higher is better.

6. Results

6.1. RQ1: Validation of LLM-in-the-loop Evaluation

First, we validate that our LLM-in-the-loop evaluator reproduces a key qualitative pattern of substantive fairness reported in prior human-in-the-loop experiments. Due to the cost of human evaluation, Cresswell et al. (2025) only evaluated two CP methods, Marginal and Mondrian, on three datasets, FACET, BiosBias, and RAVDESS. They found that Mondrian CP induced greater disparate impact on downstream prediction accuracy compared to Marginal.

In Table 2 we compare **maxROR** measurements between the human experiment data collected by Cresswell et al. (2025), and with our LLM evaluator. LLM-in-the-loop consistently reproduces the qualitative **maxROR** ordering for Marginal and Mondrian CP, with Mondrian showing greater unfairness across all three datasets. This consistency supports the use of our LLM-in-the-loop evaluator as a scalable proxy for diagnosing substantive fairness trends and rankings across CP methods. See Appendix E.1 for further calibration details of the LLM-in-the-loop evaluator.

6.2. RQ2: Substantive Fairness Benchmarking

Having verified that our LLM-in-the-loop evaluator has similar qualitative behaviour to human decision-makers, we address the question: *Which CP methods are most fair*

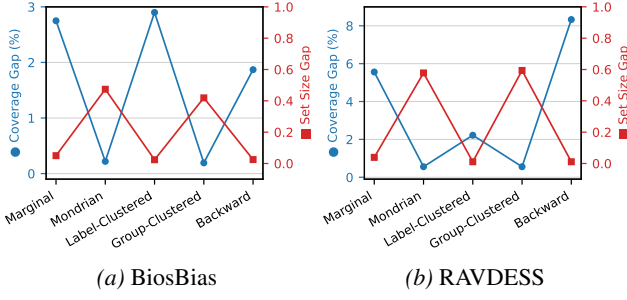


Figure 3. Coverage gap (blue dots, left axis) and set size gap (red squares, right axis) across CP methods. The two procedural fairness metrics are in direct tension. Corresponding plots for FACET and ACSIncome are in Appendix F.

in downstream tasks? We again measure the **maxROR** metric, but cover a wider variety of CP methods and datasets than prior research. In addition, sets should be helpful as a decision aid, so we also consider the overall accuracy of the LLM-in-the-loop on its task, relative to the control where no prediction set is provided. Our results in Figure 1 identify **Backward and Label-Clustered CP as the most substantively fair** methods on average, but also that Label-Clustered CP is the more helpful of the two (Figure 2).

On FACET and BiosBias, Backward CP achieved the lowest **maxROR**. However, Backward CP suffers from larger set size than other CP methods, partially due to its conservative empirical coverage (Table 1), and hence also is less helpful for the task as seen by lower accuracy improvement in all comparisons. Meanwhile, Label-Clustered CP offers a robust balance between efficiency and substantive fairness. Its **maxROR** was considerably lower than Backward on RAVDESS and ACSIncome, with much greater helpfulness to the decision maker.

In contrast, Mondrian and Group-Clustered CP are never optimal in terms of **maxROR** and induced by far the most unfair outcomes for FACET and RAVDESS. For BiosBias they lead to the highest accuracy improvements, but clearly these improvements are not shared equally across groups in the data. Mondrian and Group-Clustered CP by design equalize coverage across groups, but this may be in opposition to downstream equity.

Extended details on these experiments are in Appendix E.2, including an ablation with a different LLM on BiosBias.

6.3. RQ3: Procedural and Substantive Correlations

Next, we ask: *Which procedural fairness metric correlates most strongly with substantive fairness?* Traditionally, researchers have focused on minimizing the coverage gap (Romano et al., 2020a), with more recent studies recommending set size gap as an alternative (Cresswell et al., 2025). Figure 3 demonstrates that these two procedural met-

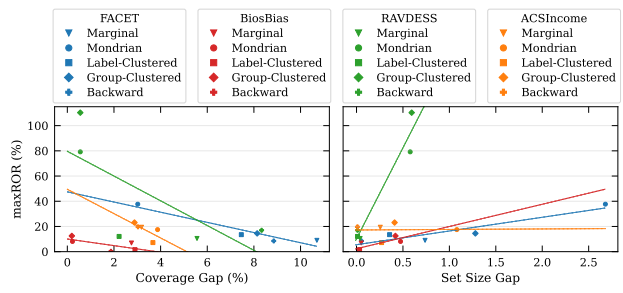


Figure 4. **maxROR** (%) compared to the coverage gap (Left) and set size gap (Right) between groups, across CP methods and datasets. Regression lines are fitted for each dataset individually to show trends.

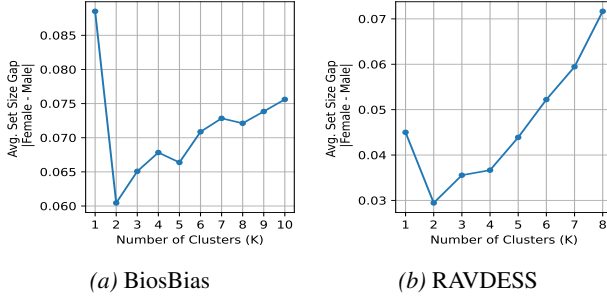
rics are in diametric opposition; CP methods optimize one at the expense of the other. Understanding which of these metrics correlates with substantive fairness enables its use as an early diagnostic signal of unfairness before expensive downstream deployments are undertaken.

In Figure 4 we plot the procedural fairness metrics against our substantive metric, **maxROR** for each dataset and CP method. Since the metrics are on different scales between datasets, we also plot individual regression lines for the data from each dataset. We clearly see that all four regressions for the coverage gap have negative slope; decreasing the coverage gap (equalizing coverage between groups) leads to higher **maxROR** (greater unfairness). The set size gap data on the other hand shows positive slopes, such that decreasing it (equalizing set size) also decreases **maxROR**. From these consistent trends across datasets it is evident that Equalized Set Size as a procedural fairness notion is also aligned with substantive fairness goals of downstream equity, whereas Equalized Coverage is actively inequitable.

6.4. RQ4: Effect of Label-Clustered CP on Set Size Gap

Knowing that set size gap is a relevant predictor of downstream fairness, we revisit our theoretical analysis from Section 4.1 and verify its insights experimentally. In Theorem 4.1 we decomposed the set size disparity $\Delta_{a,b}$ (Equation (14)) into three components that are affected by label clusters and groups in the data. We now examine the behaviour of the bound overall, the interplay of the three terms, and the effect of Label-Clustered CP’s main hyperparameter—the number of clusters K .

First, using the BiosBias and RAVDESS datasets in Figure 5, we vary the number of clusters from $K = 1$ (Marginal CP) up to the total number of classes m , and compute the average set size gap for Label-Clustered CP over 10 random calibration-test splits. The observed relationship between K and $\Delta_{a,b}$ exhibits a clear V-shaped pattern with a minimum of set size disparity at $K = 2$, and sharp increase for $K = 1$. This connects back to Label-Clustered CP’s ability to reduce



(a) BiosBias

(b) RAVDESS

Figure 5. Average prediction set size gap between Female and Male on the BiosBias and RAVDESS datasets over 10 random splits. The maximum standard error of the average set size gap is .016 in (a) and .010 in (b).

substantive unfairness compared to Marginal (Figure 1) by reducing the set size gap; clustering combines datapoints with similar labels regardless of group such that model confidence can be calibrated accurately within the clusters.

We show more detail on the behaviour of the three terms separately for RAVDESS in Figure 6. While term III is generally the largest and gives rise to the distinctive V shape with a minimum at $K = 2$, the other terms’ behavior closely aligns with the discussion in Section 4.1. When $K = 1$ (Marginal CP), term II, the cross-cluster spread of expected set sizes, is of course minimized, but term I remains large due to substantial label heterogeneity within the single cluster. Increasing K reduces intra-cluster label heterogeneity I, while the cross-cluster spread II increases as calibration becomes less stable for small clusters.

Finally, in Figure 7 we demonstrate the tightness of the bound on RAVDESS by numerically computing $\Delta_{a,b}$ vs. the sum of all three terms. The bound is reasonably tight, demonstrating a regular and small bias, allowing us to rely on the interpretations of the three individual terms.

Overall, these experiments validate the theoretical statement that, with a carefully chosen number of clusters, Label-Clustered CP can more effectively balance label adaptivity and calibration stability to improve set size disparity, which correlates strongly with substantive fairness. Our decomposition gives insight into *why* Label-Clustered CP is able to achieve better procedural fairness (Equalized Set Size) than other CP methods (Figure 3), and by extension better substantive fairness (Figure 1).

6.5. Practical Guidelines

Based on these theoretical and empirical findings, we offer the following recommendations for deploying CP in fairness-critical decision pipelines:

Evaluate both procedural and substantive fairness: Equality and equity are both noble pursuits, but can sometimes be at odds (Figure 4 left). Determine which criteria

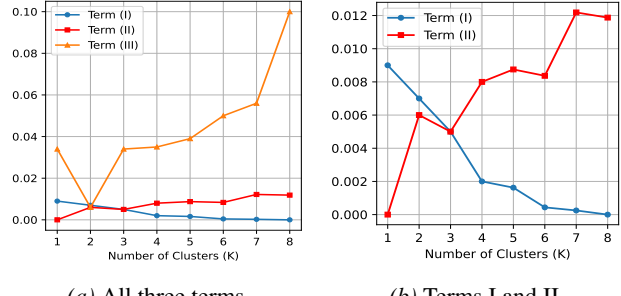


Figure 6. Numerical computation of the three terms in Equation (13) vs. number of clusters K on RAVDESS.

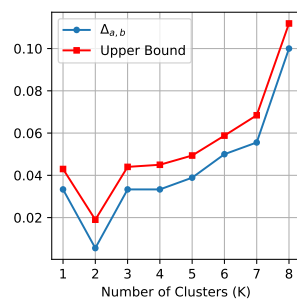


Figure 7. Numerical computation of $\Delta_{a,b}$ vs. the upper bound from Equation (13) on RAVDESS with Label-Clustered CP. The bound is reasonably tight and faithfully reflects the shape of $\Delta_{a,b}$ as K is varied.

cannot be compromised on prior to building CP systems, and evaluate metrics reflecting both notions throughout development.

Prioritize minimizing set size gaps: Do not optimize for Equalized Coverage in isolation. Equalized Set Size correlates strongly with substantive fairness, whereas equalizing coverage tends to increase **maxROR** (Figure 4).

Avoid demographic conditioning: Methods that explicitly condition on the protected group (e.g., Mondrian, Group-Clustered) tend to amplify set size disparity to satisfy coverage constraints. Instead, conditioning on labels (Label-Clustered CP) calibrates thresholds within clusters of similar difficulty, which naturally balances sets without baking in group biases.

7. Conclusion

In this work, we moved beyond the view of conformal prediction as a standalone procedure, and evaluated its impact on *substantive fairness* in downstream decision-making. By designing a scalable LLM-in-the-loop evaluator, we demonstrated that the standard procedural fairness notion, Equalized Coverage, often fails to translate into equitable outcomes. Instead, our findings highlight that equalizing set size is the critical procedural lever that correlates with substantive fairness, with Label-Clustered CP achieving the

most effective balance of utility and equity.

A promising avenue for future work is to deepen the causal analysis of these interactions. While our current study identifies strong correlations, explicitly controlling the **adoption rate** of the LLM evaluator (systematically varying how much the agent relies on the prediction set) would allow for a rigorous isolation of the causal effects of set properties on substantive decision outcomes.

Impact Statement

In this work we study the interactions between uncertainty quantification methods and fairness, pointing out a gap in the way fairness has been quantified in previous studies. The impact of our work is to raise awareness on issues of equity in machine learning, and as such we do not expect negative societal impacts to arise.

References

Akiba, T., Sano, S., Yanase, T., Ohta, T., and Koyama, M. Optuna: A next-generation hyperparameter optimization framework. In *Proceedings of the 25th ACM SIGKDD international conference on knowledge discovery & data mining*, pp. 2623–2631, 2019. [27](#)

Angelopoulos, A. N. and Bates, S. A gentle introduction to conformal prediction and distribution-free uncertainty quantification. *arXiv:2107.07511*, 2021. [1](#)

Angelopoulos, A. N., Bates, S., Jordan, M., and Malik, J. Uncertainty sets for image classifiers using conformal prediction. In *International Conference on Learning Representations*, 2021. [2](#), [26](#)

Baevski, A., Zhou, Y., Mohamed, A., and Auli, M. wav2vec 2.0: A Framework for Self-Supervised Learning of Speech Representations. In *Advances in Neural Information Processing Systems*, volume 33, pp. 12449–12460, 2020. [6](#), [25](#)

Bai, S., Chen, K., Liu, X., Wang, J., Ge, W., Song, S., Dang, K., Wang, P., Wang, S., Tang, J., Zhong, H., Zhu, Y., Yang, M., Li, Z., Wan, J., Wang, P., Ding, W., Fu, Z., Xu, Y., Ye, J., Zhang, X., Xie, T., Cheng, Z., Zhang, H., Yang, Z., Xu, H., and Lin, J. Qwen2.5-VL Technical Report. *arXiv:2502.13923*, 2025. [5](#)

Barocas, S., Hardt, M., and Narayanan, A. *Fairness and machine learning: Limitations and opportunities*. MIT press, 2023. [1](#)

Berk, R. A., Kuchibhotla, A. K., and Tchetgen, E. T. Improving fairness in criminal justice algorithmic risk assessments using optimal transport and conformal prediction sets. *Sociological Methods & Research*, 2023. doi: 10.1177/00491241231155883. [3](#)

Buolamwini, J. and Gebru, T. Gender Shades: Intersectional Accuracy Disparities in Commercial Gender Classification. In *Proceedings of the 1st Conference on Fairness, Accountability and Transparency*, volume 81, pp. 77–91, 2018. [25](#)

Chen, T. and Guestrin, C. XGBoost: A Scalable Tree Boosting System. In *Proceedings of the 22nd ACM SIGKDD International Conference on Knowledge Discovery and Data Mining*, pp. 785–794, 2016. ISBN 9781450342322. doi: 10.1145/2939672.2939785. [6](#), [25](#)

Cresswell, J. C. Trustworthy AI Must Account for Interactions. *arXiv:2504.07170*, 2025. [1](#)

Cresswell, J. C., Sui, Y., Kumar, B., and Vouitsis, N. Conformal prediction sets improve human decision making. In *Proceedings of the 41st International Conference on Machine Learning*, 2024. [2](#)

Cresswell, J. C., Kumar, B., Sui, Y., and Belbahri, M. Conformal prediction sets can cause disparate impact. In *The Thirteenth International Conference on Learning Representations*, 2025. [2](#), [3](#), [4](#), [6](#), [7](#), [22](#), [31](#)

De-Arteaga, M., Romanov, A., Wallach, H., Chayes, J., Borgs, C., Chouldechova, A., Geyik, S., Kenthapadi, K., and Kalai, A. T. Bias in Bios: A Case Study of Semantic Representation Bias in a High-Stakes Setting. In *Proceedings of the Conference on Fairness, Accountability, and Transparency*, pp. 120–128, 2019. ISBN 9781450361255. doi: 10.1145/3287560.3287572. [6](#), [25](#)

Devlin, J., Chang, M.-W., Lee, K., and Toutanova, K. BERT: Pre-training of Deep Bidirectional Transformers for Language Understanding. In *Proceedings of the 2019 Conference of the North American Chapter of the Association for Computational Linguistics: Human Language Technologies, Volume 1 (Long and Short Papers)*, pp. 4171–4186, 2019. doi: 10.18653/v1/N19-1423. [6](#), [25](#)

Ding, F., Hardt, M., Miller, J., and Schmidt, L. Retiring Adult: New Datasets for Fair Machine Learning. In *Advances in Neural Information Processing Systems*, volume 34, pp. 6478–6490, 2021. [6](#), [25](#)

Ding, T., Angelopoulos, A., Bates, S., Jordan, M., and Tibshirani, R. J. Class-conditional conformal prediction with many classes. In *Advances in Neural Information Processing Systems*, volume 36, pp. 64555–64576, 2023. [3](#), [18](#), [19](#), [27](#)

Dosovitskiy, A., Beyer, L., Kolesnikov, A., Weissenborn, D., Zhai, X., Unterthiner, T., Dehghani, M., Minderer, M., Heigold, G., Gelly, S., Uszkoreit, J., and Houlsby, N. ImageScope: A Framework for Interpreting and Debugging Vision Models. *arXiv:2306.02338*, 2023. [1](#)

N. An Image is Worth 16x16 Words: Transformers for Image Recognition at Scale. In *International Conference on Learning Representations*, 2021. 5

Drukker, K., Chen, W., Gichoya, J., Gruszauskas, N., Kalpathy-Cramer, J., Koyejo, S., Myers, K., Sá, R. C., Sahiner, B., Whitney, H., et al. Toward fairness in artificial intelligence for medical image analysis: identification and mitigation of potential biases in the roadmap from data collection to model deployment. *Journal of Medical Imaging*, 10(6):061104–061104, 2023. 25

Fadel, W. Fine-tuned XLSR-53 large model for speech emotion recognition on ravdess dataset, 2023. URL <https://huggingface.co/Wiam/wav2vec2-large-xlsr-53-english-finetuned-ravdess-v5>. Accessed 2025-10-01. 25

Foygel Barber, R., Candes, E. J., Ramdas, A., and Tibshirani, R. J. The limits of distribution-free conditional predictive inference. *Information and Inference: A Journal of the IMA*, 10(2):455–482, 2021. 3, 16

Gal, Y. and Ghahramani, Z. Dropout as a Bayesian Approximation: Representing Model Uncertainty in Deep Learning. In *Proceedings of The 33rd International Conference on Machine Learning*, volume 48, pp. 1050–1059, 2016. 1

Garcia-Galindo, A., Lopez-De-Castro, M., and Armananzas, R. Fair prediction sets through multi-objective hyperparameter optimization. *Machine Learning*, 114(1):27, 2025. 3

Gauthier, E., Bach, F., and Jordan, M. I. Backward conformal prediction. In *Advances in Neural Information Processing Systems*, volume 38, 2025. 3, 19

Gibbs, I., Cherian, J. J., and Candès, E. J. Conformal prediction with conditional guarantees. *Journal of the Royal Statistical Society Series B: Statistical Methodology*, 87(4):1100–1126, 2025. ISSN 1369-7412. doi: 10.1093/rssb/qkaf008. 2

Grattafiori, A. et al. The Llama 3 Herd of Models. *arXiv:2407.21783*, 2024. 32

Green, B. Escaping the impossibility of fairness: From formal to substantive algorithmic fairness. *Philosophy & Technology*, 35(4):90, 2022. 2

Grosman, J. Fine-tuned XLSR-53 large model for speech recognition in English. <https://huggingface.co/jonatasgrosman/wav2vec2-large-xlsr-53-english>, 2021. 25

Guldogan, O., Sarna, N., Li, Y., and Berger, M. Counterfactually fair conformal prediction. *arXiv:2510.08724*, 2025. 3

Gustafson, L., Rolland, C., Ravi, N., Duval, Q., Adcock, A., Fu, C.-Y., Hall, M., and Ross, C. FACET: Fairness in computer vision evaluation benchmark. In *Proceedings of the IEEE/CVF International Conference on Computer Vision*, pp. 20370–20382, 2023. 5, 25

Hardt, M., Price, E., and Srebro, N. Equality of Opportunity in Supervised Learning. In *Advances in Neural Information Processing Systems*, volume 29, 2016. 1, 2

Huang, J., Xi, H., Zhang, L., Yao, H., Qiu, Y., and Wei, H. Conformal prediction for deep classifier via label ranking. In *Proceedings of the 41st International Conference on Machine Learning*, volume 235, pp. 20331–20347, 2024. 2, 26

Kuchibhotla, A. K. and Berk, R. A. Nested conformal prediction sets for classification with applications to probation data. *The Annals of Applied Statistics*, 17(1):761–785, 2023. 3

Kusner, M. J., Loftus, J., Russell, C., and Silva, R. Counterfactual fairness. In *Advances in Neural Information Processing Systems*, volume 30, 2017. 1, 3

Lakshminarayanan, B., Pritzel, A., and Blundell, C. Simple and scalable predictive uncertainty estimation using deep ensembles. In *Advances in Neural Information Processing Systems*, volume 30, 2017. 1

Lei, J., Robins, J., and Wasserman, L. Distribution-free prediction sets. *Journal of the American Statistical Association*, 108(501):278–287, 2013. doi: 10.1080/01621459.2012.751873. 3

Liang, K.-Y. and Zeger, S. L. Longitudinal data analysis using generalized linear models. *Biometrika*, 73(1):13–22, 1986. 5

Liu, M., Ding, L., Yu, D., Liu, W., Kong, L., and Jiang, B. Conformalized fairness via quantile regression. In *Advances in Neural Information Processing Systems*, volume 35, 2022. 3

Livingstone, S. R. and Russo, F. A. The Ryerson Audio-Visual Database of Emotional Speech and Song (RAVDESS), April 2018. URL <https://doi.org/10.5281/zenodo.1188976>. 6, 25

Lu, C., Lemay, A., Chang, K., Höbel, K., and Kalpathy-Cramer, J. Fair conformal predictors for applications in medical imaging. In *Proceedings of the AAAI Conference on Artificial Intelligence*, volume 36, pp. 12008–12016, 2022. 3

Neal, R. M. *Bayesian learning for neural networks*, volume 118. Springer Science & Business Media, 2012. 1

Office of the Comptroller of the Currency. Fair lending, 2026. URL <https://www.occ.treas.gov/topics/consumers-and-communities/consumer-protection/fair-lending/index-fair-lending.htm>. Accessed: 2026-01-25. 2

OpenAI. GPT-4o mini: advancing cost-efficient intelligence, 2024. URL <https://openai.com/index/gpt-4o-mini-advancing-cost-efficient-intelligence/>. Accessed: 2026-01-26. 6

OpenAI. Gpt-4o audio model, 2026. URL <https://platform.openai.com/docs/models/gpt-4o-audio-preview>. Accessed: 2026-01-26. 6

Radford, A., Kim, J. W., Hallacy, C., Ramesh, A., Goh, G., Agarwal, S., Sastry, G., Askell, A., Mishkin, P., Clark, J., Krueger, G., and Sutskever, I. Learning Transferable Visual Models From Natural Language Supervision. In *Proceedings of the 38th International Conference on Machine Learning*, volume 139, pp. 8748–8763, 2021. 5, 25

Romano, Y., Barber, R. F., Sabatti, C., and Candès, E. With Malice Toward None: Assessing Uncertainty via Equalized Coverage. *Harvard Data Science Review*, 2(2), 2020a. 1, 2, 3, 7

Romano, Y., Sesia, M., and Candes, E. Classification with valid and adaptive coverage. In *Advances in Neural Information Processing Systems*, volume 33, pp. 3581–3591, 2020b. 2

Shafer, G. and Vovk, V. A tutorial on conformal prediction. *Journal of Machine Learning Research*, 9(3), 2008. 1

Srinivasan, A., Vadlamani, A. T., Meghrazi, A., and Parthasarathy, S. FedCF: Fair Federated Conformal Prediction. *arXiv:2509.22907*, 2025. 3

Tasar, D. E. The coverage-deferral trade-off: Fairness implications of conformal prediction in human-in-the-loop decision systems. *Preprints*, 2025. doi: 10.20944/preprints202512.2631.v1. 3

Vadlamani, A. T., Srinivasan, A., Maneriker, P., Payani, A., and Parthasarathy, S. A generic framework for conformal fairness. In *The Thirteenth International Conference on Learning Representations*, 2025. 3

Vovk, V. Conditional validity of inductive conformal predictors. In *Proceedings of the Asian Conference on Machine Learning*, volume 25, pp. 475–490, 2012. 3, 16

Vovk, V. Conformal e-prediction. *Pattern Recognition*, 166: 111674, 2025. ISSN 0031-3203. doi: 10.1016/j.patcog.2025.111674. 3

Vovk, V., Gammerman, A., and Saunders, C. Machine-learning applications of algorithmic randomness. In *Proceedings of the Sixteenth International Conference on Machine Learning*, pp. 444–453, 1999. 2

Vovk, V., Lindsay, D., Nouretdinov, I., and Gammerman, A. Mondrian confidence machine. *Technical Report*, 2003. 2

Vovk, V., Gammerman, A., and Shafer, G. *Algorithmic Learning in a Random World*. Springer New York, 2005. doi: 10.1007/b106715. 1, 2, 16

Wang, F., Cheng, L., Guo, R., Liu, K., and Yu, P. S. Equal opportunity of coverage in fair regression. *Advances in Neural Information Processing Systems*, 36, 2024. 3

Yang, A., Yang, B., Zhang, B., Hui, B., Zheng, B., Yu, B., Li, C., Liu, D., Huang, F., Wei, H., Lin, H., Yang, J., Tu, J., Zhang, J., Yang, J., Yang, J., Zhou, J., Lin, J., Dang, K., Lu, K., Bao, K., Yang, K., Yu, L., Li, M., Xue, M., Zhang, P., Zhu, Q., Men, R., Lin, R., Li, T., Tang, T., Xia, T., Ren, X., Ren, X., Fan, Y., Su, Y., Zhang, Y., Wan, Y., Liu, Y., Cui, Z., Zhang, Z., and Qiu, Z. Qwen2.5 Technical Report. *arXiv:2412.15115*, 2024a. 6

Yang, J., Jiang, J., Sun, Z., and Chen, J. A large-scale empirical study on improving the fairness of image classification models. In *Proceedings of the 33rd ACM SIGSOFT International Symposium on Software Testing and Analysis*, pp. 210–222, 2024b. 25

Zemel, R., Wu, Y., Swersky, K., Pitassi, T., and Dwork, C. Learning fair representations. In *Proceedings of the 30th International Conference on Machine Learning*, volume 28, pp. 325–333, 2013. 1

Zerva, C. and Martins, A. F. T. Conformalizing machine translation evaluation. *Transactions of the Association for Computational Linguistics*, 12:1460–1478, 2024. doi: 10.1162/tacl_a_00711. 3

Zhou, Y. and Sesia, M. Conformal classification with equalized coverage for adaptively selected groups. In *Advances in Neural Information Processing Systems*, volume 37, 2024. doi: 10.52202/079017-3454. 3

Zwart, P. H. Probabilistic conformal coverage guarantees in small-data settings. *arXiv:2509.15349*, 2025. 2

Appendix

Table of Contents

A Justification that Label-Clustered CP Reduces Set Size Disparity	12
B Conformal Prediction Algorithms	19
B.1 Clustered Conformal Prediction	19
B.2 Backward Conformal Prediction	19
B.3 Pseudocode Implementations	19
C Technical Details of the LLM-in-the-loop Evaluator	22
C.1 Constructing GEE to Predict Downstream Prediction Accuracy	22
C.2 Measuring Substantive Fairness from the LLM-in-the-loop Evaluator	23
D Additional Experiment Details	25
D.1 Dataset Details	25
D.2 Score Functions Used for Conformal Prediction	26
D.3 Hyperparameters	27
D.4 Prompts Used for LLM-in-the-loop Evaluator	28
E Details and Results from the LLM-in-the-loop Evaluator	31
E.1 Comparing Human-in-the-loop and LLM-in-the-loop Evaluators	31
E.2 LLM-in-the-loop Evaluator Results on Different Tasks	32
E.3 Bootstrap Results	33
F Additional Tables and Plots	35
F.1 CP and LLM-in-the-loop Metrics by Group	35
F.2 Additional Coverage Gap and Set Size Gap Plots	40

A. Justification that Label-Clustered CP Reduces Set Size Disparity

In this appendix, we provide justification on how Label-Clustered CP reduces set size gap between protected *groups*, even though it does calibration based on clusters of *labels*. Let A be the random variable of the protected groups, that is, the possible values of A are all protected groups. Consider any two protected groups, say group a and group b , we want to show that the gap between $\mathbb{E}[|\mathcal{C}(X)| \mid A = a]$ and $\mathbb{E}[|\mathcal{C}(X)| \mid A = b]$ can be reduced by implementing Label-Clustered CP, improving fairness between group a and group b in terms of prediction set size, especially compared to Mondrian CP. In what follows, $\mathcal{C}(X)$ denotes the prediction set constructed from Label-Clustered CP, and $|\mathcal{C}(X)|$ is the cardinality of the prediction set $\mathcal{C}(X)$.

Proof of Theorem 4.1: According to the law of total expectation, we have

$$\mathbb{E}[|\mathcal{C}(X)| \mid A = a] = \sum_{y \in \mathcal{Y}} \mathbb{P}(Y = y \mid A = a) \mathbb{E}[|\mathcal{C}(X)| \mid Y = y, A = a]$$

$$\mathbb{E}[|\mathcal{C}(X)| \mid A = b] = \sum_{y \in \mathcal{Y}} \mathbb{P}(Y = y \mid A = b) \mathbb{E}[|\mathcal{C}(X)| \mid Y = y, A = b]$$

Let $\Delta_{a,b} = |\mathbb{E}[|\mathcal{C}(X)| \mid A = a] - \mathbb{E}[|\mathcal{C}(X)| \mid A = b]|$ be the disparity in expected set size, so we have

$$\begin{aligned} \Delta_{a,b} &= \left| \sum_{y \in \mathcal{Y}} \mathbb{P}(Y = y \mid A = a) \mathbb{E}[|\mathcal{C}(X)| \mid Y = y, A = a] - \sum_{y \in \mathcal{Y}} \mathbb{P}(Y = y \mid A = b) \mathbb{E}[|\mathcal{C}(X)| \mid Y = y, A = b] \right. \\ &\quad \left. + \sum_{y \in \mathcal{Y}} \mathbb{P}(Y = y \mid A = a) \mathbb{E}[|\mathcal{C}(X)| \mid Y = y, A = b] - \sum_{y \in \mathcal{Y}} \mathbb{P}(Y = y \mid A = a) \mathbb{E}[|\mathcal{C}(X)| \mid Y = y, A = b] \right| \\ &= \left| \underbrace{\sum_{y \in \mathcal{Y}} [\mathbb{P}(Y = y \mid A = a) - \mathbb{P}(Y = y \mid A = b)] \mathbb{E}[|\mathcal{C}(X)| \mid Y = y, A = b]}_{(I)} \right. \\ &\quad \left. + \underbrace{\sum_{y \in \mathcal{Y}} \mathbb{P}(Y = y \mid A = a) \{ \mathbb{E}[|\mathcal{C}(X)| \mid Y = y, A = a] - \mathbb{E}[|\mathcal{C}(X)| \mid Y = y, A = b] \}}_{(II)} \right| \end{aligned} \quad (\text{A1})$$

$$\quad (\text{A2})$$

We analyze term (I) in Equation (A1) and term (II) in Equation (A2) individually to investigate how Label-Clustered CP controls the gap of expected set size between group a and group b . Recall the clustering function $h : \mathcal{Y} \rightarrow \{1, \dots, K\}$ that maps each class $y \in \mathcal{Y}$ to one of the K clusters based on score distributions of the labels. Throughout the arguments in this appendix, we treat h as fixed by conditioning on the portion of data (clustering data set) used to learn it. Let $\mathcal{Y}_k := \{y \in \mathcal{Y} : h(y) = k\}$ be the set of labels in the k -th cluster for each $k = 1, \dots, K$. Then,

$$\begin{aligned} (I) &= \sum_{y \in \mathcal{Y}} [\mathbb{P}(Y = y \mid A = a) - \mathbb{P}(Y = y \mid A = b)] \mathbb{E}[|\mathcal{C}(X)| \mid Y = y, A = b] \\ &= \sum_{k=1}^K \sum_{y \in \mathcal{Y}_k} [\mathbb{P}(Y = y \mid A = a) - \mathbb{P}(Y = y \mid A = b)] \mathbb{E}[|\mathcal{C}(X)| \mid Y = y, A = b] \\ &= \sum_{k=1}^K \sum_{y \in \mathcal{Y}_k} [\mathbb{P}(Y = y, h(Y) = h(y) \mid A = a) - \mathbb{P}(Y = y, h(Y) = h(y) \mid A = b)] \cdot \mathbb{E}[|\mathcal{C}(X)| \mid Y = y, A = b] \\ &\quad (\text{because } Y = y \Rightarrow h(Y) = h(y)) \\ &= \sum_{k=1}^K \sum_{y \in \mathcal{Y}_k} [\mathbb{P}(Y = y, h(Y) = k \mid A = a) - \mathbb{P}(Y = y, h(Y) = k \mid A = b)] \cdot \mathbb{E}[|\mathcal{C}(X)| \mid Y = y, A = b] \\ &= \sum_{k=1}^K \mathbb{P}(h(Y) = k \mid A = a) \sum_{y \in \mathcal{Y}_k} \mathbb{P}(Y = y \mid h(Y) = k, A = a) \mathbb{E}[|\mathcal{C}(X)| \mid Y = y, A = b] \\ &\quad - \sum_{k=1}^K \mathbb{P}(h(Y) = k \mid A = b) \sum_{y \in \mathcal{Y}_k} \mathbb{P}(Y = y \mid h(Y) = k, A = b) \mathbb{E}[|\mathcal{C}(X)| \mid Y = y, A = b] \end{aligned}$$

Now, define

$$\begin{aligned} (I)_1 &:= \sum_{k=1}^K \mathbb{P}(h(Y) = k \mid A = a) \sum_{y \in \mathcal{Y}_k} \mathbb{P}(Y = y \mid h(Y) = k, A = a) \mathbb{E}[|\mathcal{C}(X)| \mid Y = y, A = b] \\ &\quad - \sum_{k=1}^K \mathbb{P}(h(Y) = k \mid A = a) \sum_{y \in \mathcal{Y}_k} \mathbb{P}(Y = y \mid h(Y) = k, A = b) \mathbb{E}[|\mathcal{C}(X)| \mid Y = y, A = b] \end{aligned}$$

and

$$\begin{aligned} (I)_2 &:= \sum_{k=1}^K \mathbb{P}(h(Y) = k \mid A = a) \sum_{y \in \mathcal{Y}_k} \mathbb{P}(Y = y \mid h(Y) = k, A = b) \mathbb{E}[|\mathcal{C}(X)| \mid Y = y, A = b] \\ &\quad - \sum_{k=1}^K \mathbb{P}(h(Y) = k \mid A = b) \sum_{y \in \mathcal{Y}_k} \mathbb{P}(Y = y \mid h(Y) = k, A = b) \mathbb{E}[|\mathcal{C}(X)| \mid Y = y, A = b] \end{aligned}$$

Then, we have $(I) = (I)_1 + (I)_2$. We analyze $(I)_1$ and $(I)_2$ separately as follows.

1. Bound $|(I)_1|$:

We can rewrite $(I)_1$ as

$$(I)_1 = \sum_{k=1}^K \mathbb{P}(h(Y) = k | A = a) \sum_{y \in \mathcal{Y}_k} [\mathbb{P}(Y = y | h(Y) = k, A = a) - \mathbb{P}(Y = y | h(Y) = k, A = b)] \mathbb{E}[|\mathcal{C}(X)| | Y = y, A = b] \quad (\text{A3})$$

First, fix a cluster k . Since $\sum_{y \in \mathcal{Y}_k} \mathbb{P}(Y = y | h(Y) = k, A = a) - \mathbb{P}(Y = y | h(Y) = k, A = b) = 0$, for any constant c , we have

$$\begin{aligned} & \sum_{y \in \mathcal{Y}_k} [\mathbb{P}(Y = y | h(Y) = k, A = a) - \mathbb{P}(Y = y | h(Y) = k, A = b)] \mathbb{E}[|\mathcal{C}(X)| | Y = y, A = b] \\ &= \sum_{y \in \mathcal{Y}_k} [\mathbb{P}(Y = y | h(Y) = k, A = a) - \mathbb{P}(Y = y | h(Y) = k, A = b)] (\mathbb{E}[|\mathcal{C}(X)| | Y = y, A = b] - c) \end{aligned}$$

Applying this logic, if we define $c_k := \frac{1}{2} (\max_{y \in \mathcal{Y}_k} \mathbb{E}[|\mathcal{C}(X)| | Y = y, A = b] + \min_{y \in \mathcal{Y}_k} \mathbb{E}[|\mathcal{C}(X)| | Y = y, A = b])$, then we have

$$\begin{aligned} & \left| \sum_{y \in \mathcal{Y}_k} [\mathbb{P}(Y = y | h(Y) = k, A = a) - \mathbb{P}(Y = y | h(Y) = k, A = b)] \mathbb{E}[|\mathcal{C}(X)| | Y = y, A = b] \right| \\ &= \left| \sum_{y \in \mathcal{Y}_k} [\mathbb{P}(Y = y | h(Y) = k, A = a) - \mathbb{P}(Y = y | h(Y) = k, A = b)] (\mathbb{E}[|\mathcal{C}(X)| | Y = y, A = b] - c_k) \right| \\ &\leq \|\mathbf{p}_{k,a} - \mathbf{p}_{k,b}\|_1 \cdot \max_{y \in \mathcal{Y}_k} |\mathbb{E}[|\mathcal{C}(X)| | Y = y, A = b] - c_k| \quad \text{by Hölder's inequality} \\ &= \|\mathbf{p}_{k,a} - \mathbf{p}_{k,b}\|_1 \cdot \frac{1}{2} \left(\max_{y \in \mathcal{Y}_k} \mathbb{E}[|\mathcal{C}(X)| | Y = y, A = b] - \min_{y \in \mathcal{Y}_k} \mathbb{E}[|\mathcal{C}(X)| | Y = y, A = b] \right) \\ &\leq \frac{1}{2} (\|\mathbf{p}_{k,a}\|_1 + \|\mathbf{p}_{k,b}\|_1) \left(\max_{y \in \mathcal{Y}_k} \mathbb{E}[|\mathcal{C}(X)| | Y = y, A = b] - \min_{y \in \mathcal{Y}_k} \mathbb{E}[|\mathcal{C}(X)| | Y = y, A = b] \right) \quad \text{by triangle inequality} \\ &= \frac{1}{2} \cdot 2 \left(\max_{y \in \mathcal{Y}_k} \mathbb{E}[|\mathcal{C}(X)| | Y = y, A = b] - \min_{y \in \mathcal{Y}_k} \mathbb{E}[|\mathcal{C}(X)| | Y = y, A = b] \right) \\ &= \max_{y \in \mathcal{Y}_k} \mathbb{E}[|\mathcal{C}(X)| | Y = y, A = b] - \min_{y \in \mathcal{Y}_k} \mathbb{E}[|\mathcal{C}(X)| | Y = y, A = b], \end{aligned} \quad (\text{A4})$$

where $\mathbf{p}_{k,a}$ is the probability vector with each component being $\mathbb{P}(Y = y | h(Y) = k, A = a)$ for $y \in \mathcal{Y}_k$; similarly, $\mathbf{p}_{k,b}$ is the probability vector with each component being $\mathbb{P}(Y = y | h(Y) = k, A = b)$ for $y \in \mathcal{Y}_k$, so $\mathbf{p}_{k,a}$ and $\mathbf{p}_{k,b}$ are vectors of probabilities that depend on data distribution.

For simplicity, for every $k \in \{1, \dots, K\}$, define

$$\epsilon_{k,b} := \max_{y \in \mathcal{Y}_k} \mathbb{E}[|\mathcal{C}(X)| | Y = y, A = b] - \min_{y \in \mathcal{Y}_k} \mathbb{E}[|\mathcal{C}(X)| | Y = y, A = b].$$

That is, $\epsilon_{k,b}$ is the spread of expected set size over the labels in cluster k , conditioning on group b . Then, we have

$$\begin{aligned}
 |(I)_1| &\leq \sum_{k=1}^K \mathbb{P}(h(Y) = k | A = a) \left| \sum_{y \in \mathcal{Y}_k} [\mathbb{P}(Y = y | h(Y) = k, A = a) - \mathbb{P}(Y = y | h(Y) = k, A = b)] \mathbb{E}[|\mathcal{C}(X)| | Y = y, A = b] \right| \\
 &\leq \sum_{k=1}^K \mathbb{P}(h(Y) = k | A = a) \left(\max_{y \in \mathcal{Y}_k} \mathbb{E}[|\mathcal{C}(X)| | Y = y, A = b] - \min_{y \in \mathcal{Y}_k} \mathbb{E}[|\mathcal{C}(X)| | Y = y, A = b] \right) \quad \text{by Equation (A4)} \\
 &= \sum_{k=1}^K \epsilon_{k,b} \mathbb{P}(h(Y) = k | A = a) \\
 &\leq \max_{k=1, \dots, K} \epsilon_{k,b} \cdot \sum_{k=1}^K \mathbb{P}(h(Y) = k | A = a) \\
 &= \max_{k=1, \dots, K} \epsilon_{k,b}
 \end{aligned}$$

The above derivation shows that $|(I)_1|$ is upper bounded by the maximum intra-cluster expected set size difference across labels. When $K = 1$, the Label-Clustered CP reduces to a special case, Marginal CP. In this case, all labels fall into one cluster, and the upper bound for $|(I)_1|$ becomes $\epsilon_{1,b}$. Because Marginal CP does not learn the cluster assignments according to score distributions of labels, instead forcing all labels into a single cluster, the $\epsilon_{1,b}$ term can be large due to label heterogeneity. In contrast, when $K = |\mathcal{Y}|$, each label forms a cluster, and $\epsilon_{k,b} = 0$ for all $k = 1, \dots, K$, yielding $(I)_1 = 0$. Label-Clustered CP clusters labels using similarity of score distribution, which can be viewed as a proxy for label difficulty. Therefore, with a proper choice of K and the associated cluster assignment, the labels in each cluster have similar score distributions and difficulty levels, yielding small $\epsilon_{k,b}$ for each k , which gives a tight upper bound for $|(I)_1|$. Therefore, Label-Clustered CP can effectively control $|(I)_1|$ by limiting label heterogeneity within each cluster.

2. Bound $|(I)_2|$:

After combining the common terms, we get

$$(I)_2 = \sum_{k=1}^K (\mathbb{P}(h(Y) = k | A = a) - \mathbb{P}(h(Y) = k | A = b)) \sum_{y \in \mathcal{Y}_k} \mathbb{P}(Y = y | h(Y) = k, A = b) \mathbb{E}[|\mathcal{C}(X)| | Y = y, A = b] \quad (\text{A5})$$

We can simplify the $\sum_{y \in \mathcal{Y}_k} \mathbb{P}(Y = y | h(Y) = k, A = b) \mathbb{E}[|\mathcal{C}(X)| | Y = y, A = b]$ in Equation (A5) as follows.

$$\begin{aligned}
 \sum_{y \in \mathcal{Y}_k} \mathbb{P}(Y = y | h(Y) = k, A = b) \mathbb{E}[|\mathcal{C}(X)| | Y = y, A = b] &= \sum_{y \in \mathcal{Y}_k} \mathbb{P}(Y = y | h(Y) = k, A = b) \mathbb{E}[|\mathcal{C}(X)| | Y = y, h(Y) = k, A = b] \\
 &\quad (\text{because } Y = y \Rightarrow h(Y) = h(y) = k \text{ for } y \in \mathcal{Y}_k) \\
 &= \sum_{y \in \mathcal{Y}} \mathbb{P}(Y = y | h(Y) = k, A = b) \mathbb{E}[|\mathcal{C}(X)| | Y = y, h(Y) = k, A = b] \\
 &\quad (\text{because } \mathbb{P}(Y = y | h(Y) = k, A = b) = 0 \text{ for any } y \text{ not in } \mathcal{Y}_k) \\
 &= \mathbb{E}[|\mathcal{C}(X)| | h(Y) = k, A = b] \quad (\text{by the law of total expectation})
 \end{aligned}$$

Then, plug in Equation (A5), we have

$$\begin{aligned}
 (I)_2 &= \sum_{k=1}^K (\mathbb{P}(h(Y) = k | A = a) - \mathbb{P}(h(Y) = k | A = b)) \mathbb{E}[|\mathcal{C}(X)| | h(Y) = k, A = b] \\
 &= \sum_{k=1}^K (\mathbb{P}(h(Y) = k | A = a) - \mathbb{P}(h(Y) = k | A = b)) (\mathbb{E}[|\mathcal{C}(X)| | h(Y) = k, A = b] - c) \quad \text{for any constant } c
 \end{aligned}$$

The last equality holds because

$$\begin{aligned} \sum_{k=1}^K c(\mathbb{P}(h(Y) = k|A = a) - \mathbb{P}(h(Y) = k|A = b)) &= c \left(\sum_{k=1}^K \mathbb{P}(h(Y) = k|A = a) - \sum_{k=1}^K \mathbb{P}(h(Y) = k|A = b) \right) \\ &= c \cdot (1 - 1) = 0 \end{aligned}$$

Define

$$\begin{aligned} \mathbf{p}_a &:= [\mathbb{P}(h(Y) = 1|A = a), \dots, \mathbb{P}(h(Y) = K|A = a)]^T \\ \mathbf{p}_b &:= [\mathbb{P}(h(Y) = 1|A = b), \dots, \mathbb{P}(h(Y) = K|A = b)]^T \end{aligned}$$

Then, we can bound $|(I)_2|$ as follows:

$$\begin{aligned} |(I)_2| &= \left| \sum_{k=1}^K (\mathbb{P}(h(Y) = k|A = a) - \mathbb{P}(h(Y) = k|A = b)) (\mathbb{E}[|\mathcal{C}(X)| \mid h(Y) = k, A = b] - c) \right| \\ &\leq \|\mathbf{p}_a - \mathbf{p}_b\|_1 \max_{k=1, \dots, K} |\mathbb{E}[|\mathcal{C}(X)| \mid h(Y) = k, A = b] - c| \quad \text{by H\"older's inequality} \\ &= \frac{1}{2} \|\mathbf{p}_a - \mathbf{p}_b\|_1 \left(\max_{k=1, \dots, K} \mathbb{E}[|\mathcal{C}(X)| \mid h(Y) = k, A = b] - \min_{k=1, \dots, K} \mathbb{E}[|\mathcal{C}(X)| \mid h(Y) = k, A = b] \right), \end{aligned} \quad (\text{A6})$$

where the last equality holds when we choose

$$c = \frac{1}{2} \left(\max_{k=1, \dots, K} \mathbb{E}[|\mathcal{C}(X)| \mid h(Y) = k, A = b] + \min_{k=1, \dots, K} \mathbb{E}[|\mathcal{C}(X)| \mid h(Y) = k, A = b] \right).$$

From Equation (A6), we observe that the magnitude of $|(I)_2|$ depends on the product of: (1) the difference of cluster-membership distribution between the protected groups a and b , and (2) the spread of $\mathbb{E}[|\mathcal{C}(X)| \mid h(Y) = k, A = b]$ over the clusters $k = 1, \dots, K$. The factor (1), which shows up as $\|\mathbf{p}_a - \mathbf{p}_b\|_1$ in Equation (A6), is induced by the correlation between Y and A (e.g., for the BiosBias data, there is correlation between occupation (label) and gender (protected group)). Since factor (1) is data-driven, and there is intrinsic correlation between Y and A in real-world data, we cannot control it directly by applying the Label-Clustered CP. Moreover, according to the triangle inequality, we always have $\|\mathbf{p}_a - \mathbf{p}_b\|_1 \leq 2$. On the other hand, the factor (2), $\max_{k=1, \dots, K} \mathbb{E}[|\mathcal{C}(X)| \mid h(Y) = k, A = b] - \min_{k=1, \dots, K} \mathbb{E}[|\mathcal{C}(X)| \mid h(Y) = k, A = b]$ in Equation (A6), is method-driven, and we can control it by choosing a proper number of clusters K . We provide two intuitive examples to illustrate how choice of K can affect factor (2): the first one is when $K = 1$ in which case the Label-Clustered CP reduces to Marginal CP. In this case, we have factor (2) = 0, so the bound Equation (A6) becomes 0; the second example is another extreme case when $K = |\mathcal{Y}|$, that is, the number of clusters is exactly the number of possible labels, with each label forming its own cluster. In this case, for underrepresented labels with limited calibration data, we have large prediction sets for these labels, which increases set size gap among labels, resulting in a large difference in factor (2).

In general, we do not want a large K . As indicated above, a large K tends to increase the spread of set size across clusters. On the other hand, although the choice of $K = 1$ makes the upper bound in Equation (A6) vanish to 0, it boils down to Marginal CP, which, as discussed in bounding $|(I)_1|$, leads to large intra-cluster expected set size gap across labels. Moreover, as discussed in previous literature, Marginal CP can have significant disparity in terms of coverage across protected groups or labels (Vovk et al., 2005; Vovk, 2012; Foygel Barber et al., 2021). In practice, we need to choose a proper K when implementing the Label-Clustered CP to balance intra-cluster label homogeneity (for controlling $|(I)_1|$) and cross-cluster stability (for controlling $|(I)_2|$). With a suitable value of K and its associated cluster assignments, we can bring both $|(I)_1|$ and $|(I)_2|$ to reasonably small values, achieving a tight bound for $|(I)|$.

3. How Label-Clustered CP helps to control $|(II)|$:

Finally, we show how Label-Clustered CP can reduce $|(II)|$ in Equation (A2) compared to group-conditional CP. The term (II) is a weighted sum over $y \in \mathcal{Y}$ of the intra-label set size gap between group a and group b . The differences in expected set size across protected groups after conditioning on the true label depend on how conformal thresholds are calibrated. The Mondrian CP estimates separate thresholds for each protected group, which can inflate $|(II)|$ for two reasons: (i) different thresholds impose different strictness levels across groups even within the same label, and (ii) in the case of imbalanced

calibration data across groups (e.g., group a has much more calibration data than group b which has limited calibration data), splitting calibration dataset according to groups significantly reduces calibration set size of underrepresented groups, increasing quantile estimation variance and amplifying differences in the resulting set sizes among groups. In contrast, Label-Clustered CP mitigates the aforementioned inflation by using shared cluster thresholds (with each cluster threshold being the same across protected groups) estimated from pooled calibration data. This pooling stabilizes the calibration step and removes policy differences across groups induced by calibration, so the intra-label set size gap between groups is less amplified by threshold noise, typically resulting in a smaller $|(II)|$ than group-conditional CP. Below, we provide a mathematical proof to justify why Label-Clustered CP avoids inflating $|(II)|$ compared to Mondrian CP.

In what follows, a prediction set from the Label-Clustered CP is still denoted as $\mathcal{C}(X)$. For a learned clustering function $h : \mathcal{Y} \rightarrow \{1, \dots, K\}$, let \hat{q}_k be the conformal quantile for each cluster k , $k = 1, \dots, K$. On the other hand, denote a prediction set constructed from Mondrian CP as $\mathcal{C}^{\text{group}}(X)$; let \hat{q}_a^{group} and \hat{q}_b^{group} be the conformal quantiles used in Mondrian CP for protected groups a and b , respectively. Recall that the rule for constructing $\mathcal{C}(x)$ is

$$\mathcal{C}(x) = \{y \in \mathcal{Y} : s(x, y) \leq \hat{q}_{h(y)}\}$$

and the rule for constructing $\mathcal{C}^{\text{group}}(x)$ is

$$\mathcal{C}^{\text{group}}(x) = \{y \in \mathcal{Y} : s(x, y) \leq \hat{q}_{g(x)}^{\text{group}}\},$$

where $g : \mathcal{X} \rightarrow \mathcal{A}$ is the group assignment function.

Now, for a fixed $y \in \mathcal{Y}$, a protected group $g \in \mathcal{A}$, and a threshold (quantile) q , define

$$r_{y,g}(q) := \mathbb{E}[|\mathcal{C}_q(X)| \mid Y = y, A = g], \quad (\text{A7})$$

where $\mathcal{C}_q(\cdot)$ denotes the conformal prediction set obtained when the relevant rule uses threshold q while holding everything else fixed. Furthermore, assume a mild regularity condition that changing the quantile threshold slightly cannot change the expected set size arbitrarily much. Mathematically, this assumption imposes a Lipschitz continuity on the function $r_{y,g}(\cdot)$, that is, there exists $0 \leq L_{y,g} < \infty$ such that for all q, q' ,

$$|r_{y,g}(q) - r_{y,g}(q')| \leq L_{y,g}|q - q'|. \quad (\text{A8})$$

Under Mondrian CP, consider any reference threshold q^* ,

$$\begin{aligned} |(II)^{\text{group}}| &\leq \sum_{y \in \mathcal{Y}} \mathbb{P}(Y = y \mid A = a) |\mathbb{E}[|\mathcal{C}^{\text{group}}(X)| \mid Y = y, A = a] - \mathbb{E}[|\mathcal{C}^{\text{group}}(X)| \mid Y = y, A = b]| \\ &= \sum_{y \in \mathcal{Y}} \mathbb{P}(Y = y \mid A = a) |r_{y,a}(\hat{q}_a^{\text{group}}) - r_{y,b}(\hat{q}_b^{\text{group}})| \quad \text{by definition in Equation (A7)} \\ &= \sum_{y \in \mathcal{Y}} \mathbb{P}(Y = y \mid A = a) |(r_{y,a}(q^*) - r_{y,b}(q^*)) + (r_{y,a}(\hat{q}_a^{\text{group}}) - r_{y,a}(q^*)) + (r_{y,b}(q^*) - r_{y,b}(\hat{q}_b^{\text{group}}))| \\ &\leq \sum_{y \in \mathcal{Y}} \mathbb{P}(Y = y \mid A = a) (|r_{y,a}(q^*) - r_{y,b}(q^*)| + |r_{y,a}(\hat{q}_a^{\text{group}}) - r_{y,a}(q^*)| + |r_{y,b}(q^*) - r_{y,b}(\hat{q}_b^{\text{group}})|) \\ &\leq \sum_{y \in \mathcal{Y}} \mathbb{P}(Y = y \mid A = a) (|r_{y,a}(q^*) - r_{y,b}(q^*)| + L_{y,a}|\hat{q}_a^{\text{group}} - q^*| + L_{y,b}|\hat{q}_b^{\text{group}} - q^*|) \quad \text{by Equation (A8)} \\ &= \underbrace{\sum_{y \in \mathcal{Y}} \mathbb{P}(Y = y \mid A = a) |r_{y,a}(q^*) - r_{y,b}(q^*)|}_{(II)_1} + \underbrace{\sum_{y \in \mathcal{Y}} \mathbb{P}(Y = y \mid A = a) (L_{y,a}|\hat{q}_a^{\text{group}} - q^*| + L_{y,b}|\hat{q}_b^{\text{group}} - q^*|)}_{(II)_2^{\text{group}}}, \end{aligned} \quad (\text{A9})$$

From the above derivation, term $(II)_1$ is data-driven, which comes from the difference in score distributions across protected groups conditional on $Y = y$. On the other hand, the term $(II)_2^{\text{group}}$ is induced by calibration of group-conditional CP which uses different group-specific thresholds \hat{q}_a^{group} and \hat{q}_b^{group} . Moreover, term $(II)_2^{\text{group}}$ can be further inflated in the case that the calibration set is imbalanced across groups. For example, if group b is underrepresented in the calibration set, then the

quantile estimator \hat{q}_b^{group} will have high bias and variance. Such noisy quantile estimation can lead to erratic behavior of set predictor, including large sets (Ding et al., 2023).

Under Label-Clustered CP, following the same logic of deriving Equation (A9), we have

$$\begin{aligned}
 |(II)^{\text{cluster}}| &\leq \sum_{y \in \mathcal{Y}} \mathbb{P}(Y = y | A = a) |r_{y,a}(\hat{q}_{h(y)}) - r_{y,b}(\hat{q}_{h(y)})| \\
 &\leq \sum_{y \in \mathcal{Y}} \mathbb{P}(Y = y | A = a) (|r_{y,a}(q^*) - r_{y,b}(q^*)| + |r_{y,a}(\hat{q}_{h(y)}) - r_{y,a}(q^*)| + |r_{y,b}(\hat{q}_{h(y)}) - r_{y,b}(q^*)|) \\
 &\leq \sum_{y \in \mathcal{Y}} \mathbb{P}(Y = y | A = a) (|r_{y,a}(q^*) - r_{y,b}(q^*)| + L_{y,a}|\hat{q}_{h(y)} - q^*| + L_{y,b}|\hat{q}_{h(y)} - q^*|) \\
 &= \sum_{y \in \mathcal{Y}} \mathbb{P}(Y = y | A = a) |r_{y,a}(q^*) - r_{y,b}(q^*)| \quad \text{if we set each reference } q^* = \hat{q}_{h(y)}
 \end{aligned} \tag{A10}$$

Therefore, for Label-Clustered CP, the term $(II)_2^{\text{group}}$ induced by calibration disappears because the Label-Clustered CP uses the same threshold $\hat{q}_{h(y)}$ regardless of group. In contrast, in Equation (A9), $(II)_2^{\text{group}}$ cannot be eliminated due to different \hat{q}_a^{group} and \hat{q}_b^{group} . This comparison shows that compared with group-conditional CP, which can inflate $|(II)|$ through split-calibration and group-specific quantile estimation, Label-Clustered CP enforces shared thresholds across groups within each label-cluster, thereby eliminating the inflation induced by calibration and leaving only the intrinsic intra-label cross-group disparity evaluated at a common threshold.

B. Conformal Prediction Algorithms

B.1. Clustered Conformal Prediction

Clustered conformal prediction (Ding et al., 2023) splits the calibration set into a clustering portion \mathcal{D}_1 (size $\lfloor \gamma n_{\text{cal}} \rfloor$) and a calibration portion \mathcal{D}_2 . A clustering function $h : \mathcal{Y} \rightarrow [K] \cup \{\text{null}\}$ is learned on \mathcal{D}_1 (typically by embedding labels via their empirical score quantiles and applying k -means). Independent quantiles \hat{q}_k are computed on \mathcal{D}_2 restricted to each cluster k (with null using the full marginal \mathcal{D}_2).

The prediction set is

$$\mathcal{C}(x_{\text{test}}) = \{y \in \mathcal{Y} : s(x_{\text{test}}, y) \leq \hat{q}_{h(y)}\}.$$

Clustering strategies can be designed to promote fairness by grouping labels according to protected attributes (to support underrepresented groups), empirically identified unfair subpopulations, human-defined rules, or data-driven quantile-based approaches.

B.2. Backward Conformal Prediction

Backward conformal prediction (Gauthier et al., 2025) constrains prediction-set size via a rule $\mathcal{T} : (\mathcal{X} \times \mathcal{Y})^n \times \mathcal{X} \rightarrow \{1, \dots, |\mathcal{Y}|\}$, mapping calibration data and a test input to a maximum allowable size $l = \mathcal{T}(\mathcal{D}_{\text{cal}}, x_{\text{test}})$.

It relies on *e-values*—nonnegative random variables E with $\mathbb{E}[E] \leq 1$. For a positive score function $s > 0$, the test e-value for label y is

$$E_{\text{test}}(y) = \frac{s(x_{\text{test}}, y)}{\frac{1}{n+1} \left(\sum_{i=1}^n S_i + s(x_{\text{test}}, y) \right)},$$

where $S_i = s(x_i, y_i)$. The data-dependent level $\tilde{\alpha}$ is chosen as the smallest value such that the number of labels with $E_{\text{test}}(y) < 1/\tilde{\alpha}$ does not exceed l :

$$\tilde{\alpha} = \inf \left\{ \alpha \in (0, 1) : |\{y : E_{\text{test}}(y) < 1/\alpha\}| \leq l \right\}.$$

The prediction set is

$$\mathcal{C}(x_{\text{test}}) = \{y \in \mathcal{Y} : E_{\text{test}}(y) < 1/\tilde{\alpha}\}.$$

This satisfies $|\mathcal{C}(x_{\text{test}})| \leq l$ and marginal coverage $\mathbb{P}\{y \in \mathcal{C}(x)\} \geq 1 - \mathbb{E}[\tilde{\alpha}]$.

In practice, $\mathbb{E}[\tilde{\alpha}]$ is estimated via leave-one-out estimator $\hat{\alpha}^{\text{LOO}} = \frac{1}{n} \sum_{j=1}^n \tilde{\alpha}_j$, where each $\tilde{\alpha}_j$ is computed by treating the j -th calibration point as a test observation.

B.3. Pseudocode Implementations

Algorithm 1 Marginal (Split) Conformal Prediction

Require: Calibration dataset $\mathcal{D}_{\text{cal}} = \{(x_i, y_i)\}_{i=1}^{n_{\text{cal}}}$, score function s , miscoverage level α

Ensure: Prediction set $\mathcal{C}_{\hat{q}_\alpha}(x)$

- 1: Compute calibration scores $S_i \leftarrow s(x_i, y_i)$ for all $i \in [n_{\text{cal}}]$
- 2: Compute $\tau_\alpha \leftarrow \lceil (n_{\text{cal}} + 1)(1 - \alpha) \rceil / n_{\text{cal}}$
- 3: Compute threshold $\hat{q}_\alpha \leftarrow \text{Quantile}_{\tau_\alpha}(S_1, \dots, S_{n_{\text{cal}}})$
- 4: Define prediction set

$$\mathcal{C}_{\hat{q}_\alpha}(x) = \{y \in \mathcal{Y} : s(x, y) \leq \hat{q}_\alpha\}$$

Algorithm 2 Mondrian (Group-Conditional) Conformal Prediction

Require: Calibration dataset \mathcal{D}_{cal} , grouping function $g : \mathcal{X} \rightarrow \mathcal{A}$, score function s , level α

Ensure: Group-conditional prediction set $\mathcal{C}(x)$

1: **for** each group $a \in \mathcal{A}$ **do**

2: $\mathcal{I}_a \leftarrow \{i : g(x_i) = a\}$

3: Compute scores $S_i \leftarrow s(x_i, y_i)$ for $i \in \mathcal{I}_a$

4: Compute

$$\hat{q}_\alpha^{(a)} \leftarrow \text{Quantile}_{\lceil (|\mathcal{I}_a|+1)(1-\alpha) \rceil / |\mathcal{I}_a|} (\{S_i\}_{i \in \mathcal{I}_a})$$

5: **end for**

6: Define prediction set

$$\mathcal{C}(x) = \{y \in \mathcal{Y} : s(x, y) \leq \hat{q}_\alpha^{(g(x))}\}$$

Algorithm 3 Label-Clustered Conformal Prediction

Require: Calibration data $\mathcal{D}_{\text{cal}} = \{(X_i, Y_i)\}_{i=1}^{n_{\text{cal}}}$, score function s , miscoverage level α , split ratio γ

Ensure: Prediction set $\mathcal{C}_{\text{label-cluster}}(x)$

1: Select index set $I_1 \subset [n_{\text{cal}}]$ with $|I_1| = \lfloor \gamma n_{\text{cal}} \rfloor$

2: Define clustering set $\mathcal{D}_1 = \{(X_i, Y_i) : i \in I_1\}$ and calibration set $\mathcal{D}_2 = \mathcal{D}_{\text{cal}} \setminus \mathcal{D}_1$

3: Learn label clustering function

$$h : \mathcal{Y} \rightarrow [K] \cup \{\text{null}\}$$

using \mathcal{D}_1

4: **for** each cluster $k \in [K] \cup \{\text{null}\}$ **do**

5: Define index set

$$\mathcal{I}_k \leftarrow \{i \in \mathcal{D}_2 : h(Y_i) = k\}$$

6: Compute scores $S_i \leftarrow s(X_i, Y_i)$ for $i \in \mathcal{I}_k$

7: Compute cluster quantile

$$\hat{q}_k \leftarrow \text{Quantile}_{\lceil (|\mathcal{I}_k|+1)(1-\alpha) \rceil / |\mathcal{I}_k|} (\{S_i\}_{i \in \mathcal{I}_k})$$

8: **end for**

9: Construct prediction set

$$\mathcal{C}_{\text{label-cluster}}(x) = \{y \in \mathcal{Y} : s(x, y) \leq \hat{q}_{h(y)}\}$$

Algorithm 4 Group-Clustered Conformal Prediction

Require: Calibration data $\mathcal{D}_{\text{cal}} = \{(X_i, Y_i)\}_{i=1}^{n_{\text{cal}}}$, score function s , miscoverage level α , split ratio γ

Ensure: Prediction set $\mathcal{C}_{\text{group-cluster}}(x)$

- 1: Select index set $I_1 \subset [n_{\text{cal}}]$ with $|I_1| = \lfloor \gamma n_{\text{cal}} \rfloor$
- 2: Define clustering set $\mathcal{D}_1 = \{(X_i, Y_i) : i \in I_1\}$ and calibration set $\mathcal{D}_2 = \mathcal{D}_{\text{cal}} \setminus \mathcal{D}_1$
- 3: Learn group clustering function

$$\tilde{h} : \mathcal{A} \rightarrow [K] \cup \{\text{null}\}$$

using \mathcal{D}_1

- 4: **for** each cluster $k \in [K] \cup \{\text{null}\}$ **do**
- 5: Define index set

$$\mathcal{I}_k \leftarrow \{i \in \mathcal{D}_2 : \tilde{h}(g(X_i)) = k\},$$

where $g : \mathcal{X} \rightarrow \mathcal{A}$ is the group assignment function.

- 6: Compute scores $S_i \leftarrow s(X_i, Y_i)$ for $i \in \mathcal{I}_k$
- 7: Compute cluster quantile

$$\hat{q}_k \leftarrow \text{Quantile}_{\lceil (|\mathcal{I}_k|+1)(1-\alpha) \rceil / |\mathcal{I}_k|}(\{S_i\}_{i \in \mathcal{I}_k})$$

- 8: **end for**

- 9: Construct prediction set

$$\mathcal{C}_{\text{group-cluster}}(x) = \{y \in \mathcal{Y} : s(x, y) \leq \hat{q}_{\tilde{h}(g(x))}\}$$

Algorithm 5 Backward Conformal Prediction

Require: Calibration data $\{(X_i, Y_i)\}_{i=1}^n$, score function s , size constraint rule \mathcal{T}

Ensure: Prediction set $\mathcal{C}_n^{\tilde{\alpha}}(x_{\text{test}})$

- 1: Compute calibration scores $S_i \leftarrow s(X_i, Y_i)$ for $i = 1, \dots, n$
- 2: **for** each label $y \in \mathcal{Y}$ **do**
- 3: Compute test e-value

$$E_{\text{test}}(y) \leftarrow \frac{s(x_{\text{test}}, y)}{\frac{1}{n+1} \left(\sum_{i=1}^n S_i + s(x_{\text{test}}, y) \right)}$$

- 4: **end for**

- 5: Define data-dependent level

$$\tilde{\alpha} \leftarrow \inf \left\{ \alpha \in (0, 1) : \#\{y \in \mathcal{Y} : E_{\text{test}}(y) < 1/\alpha\} \leq \mathcal{T}((X_i, Y_i)_{i=1}^n, x_{\text{test}}) \right\}$$

- 6: Construct prediction set

$$\mathcal{C}_n^{\tilde{\alpha}}(x_{\text{test}}) = \{y \in \mathcal{Y} : E_{\text{test}}(y) < 1/\tilde{\alpha}\}$$

C. Technical Details of the LLM-in-the-loop Evaluator

In this appendix, we provide details of constructing the logistic GEE model in Equation (15) and computing the substantive fairness metric **maxROR** introduced in Section 4.2.

C.1. Constructing GEE to Predict Downstream Prediction Accuracy

To assess the effects of different prediction sets on human prediction accuracy and their disparity among protected groups, Cresswell et al. (2025) conducted randomized controlled trials with human decision makers, using generalized estimating equations (GEEs) to model accuracy against treatment (CP method), protected group, and task difficulty (approximated by marginal CP set size), then computing Odds Ratios (ORs) and Ratio of Odds Ratios (ROR) for treatment effects and disparities. In our evaluator for assessing substantive fairness, we consider using LLMs as downstream task predictors. For each task, an LLM is provided with the input x , a prediction set, and its coverage guarantee, outputting a label from all possible classes; in the control case, no set is provided.

For each $x_j \in \mathcal{D}_{\text{test}}$ and prediction set $\mathcal{C}_t(x_j)$ from treatment t (Marginal, Mondrian, Label-Clustered, Group-Clustered, Backward; $t = 1, \dots, T$ including Control), the LLM makes M independent predictions (to accommodate randomness of LLM responses for the same input from setting a non-zero temperature) based on x_j , $\mathcal{C}_t(x_j)$ and its coverage guarantee. The prompts used for describing the task and asking for LLM’s prediction are provided in Appendix D. Let \hat{y}_{jt}^m be the m -th prediction and $R_{jt} = \frac{1}{M} \sum_{m=1}^M \mathbf{1}\{\hat{y}_{jt}^m = y_i\}$ be the empirical prediction accuracy. For a treatment t , the disparity of improvement in prediction accuracy (relative to Control) across protected groups can be estimated as

$$\hat{\Delta}_t = \max_{a,b \in \mathcal{A}} \left| \left(\frac{1}{n_a} \sum_{j=1}^{n_a} R_{jt} - \frac{1}{n_a} \sum_{j=1}^{n_a} R_{j,\text{Control}} \right) - \left(\frac{1}{n_b} \sum_{j=1}^{n_b} R_{jt} - \frac{1}{n_b} \sum_{j=1}^{n_b} R_{j,\text{Control}} \right) \right|, \quad (\text{A11})$$

where n_a, n_b are sizes of groups a and b , respectively. However, this estimation can be misleading due to (i) neglecting confounding factors, such as systematic variations in task difficulty and the LLM’s reliance on provided sets, and (ii) intra-task correlation of predictions across treatments (predictions made for the same task are based on the same x and similar provided sets across treatments). We thus use logistic GEE regression, adjusting for covariates and clustering by task to account for the intra-task correlation.

In our LLM-in-the-loop setting, we observe that LLMs (especially the more capable ones) frequently constrain their answer to lie inside the provided prediction set. We therefore define an “adoption” indicator, $\text{adoption} = \mathbf{1}\{\text{the LLM’s predicted label is contained in the provided set}\}$. Adoption captures the extent to which the prediction set is actually used as a decision aid, and it is strongly predictive of downstream correctness (see details in Appendix E.1). Consequently, we treat “adoption” as an outcome-relevant covariate so that estimated treatment effects compare methods at comparable levels of reliance on the prediction set, rather than conflating treatment effects with shifts in how often the LLM follows the set. As a result, the following covariates are included in the logistic GEE model: (i) treatment_t , the method used to construct the prediction set; (ii) group_j , the protected group to which x_j belongs; (iii) diff_j , the difficulty of task x_j approximated by the cardinality of the Marginal CP set; (iv) $\text{adoption}_{j,t} := \frac{1}{M} \sum_{m=1}^M \mathbf{1}\{\hat{y}_{jt}^m \in \mathcal{C}_t(x_j)\}$, the proportion of predictions that fall within the provided set $\mathcal{C}_t(x_j)$ under treatment t (with $\mathcal{C}_{\text{Control}}(x_j) = \emptyset$ yielding $\text{adoption}_{j,\text{Control}} = 0$ for each instance x_j).

Then, we fit a logistic GEE across all tasks to model the probability of correct prediction as a function of treatment, protected group, task difficulty, and adoption, using task-level clustering to account for intra-task correlation across treatments. As given in Section 4.2, the GEE is expressed as

$$\text{logit}(\mathbb{E}[R_{jt}]) \sim \text{treatment}_t \times \text{group}_j + \text{diff}_j + \text{adoption}_{j,t},$$

for $j = 1, \dots, N_{\text{test}}$ and $t = 1, \dots, T$. The $\text{logit}(x) = \log \frac{x}{1-x}$, and the $\text{treatment}_t \times \text{group}_j$ means the interaction between treatment_t and group_j .

When fitting the above GEE in Python, we set `cov_struct = Exchangeable()`, which assumes that all pairs of rows associated with the same task have the same correlation in their residuals after the mean is modeled. This is plausible because we have T outcomes (R_{j1}, \dots, R_{jT}) without natural ordering for x_j , and all these T prediction outcomes share the same latent task difficulty and information, making a common intra-task correlation a reasonable condition. Even if there is heteroskedasticity within clusters, adding `.fit(cov_type='robust')` guarantees the consistency of standard error estimation when N_{test} is large enough, protecting us against misspecifying the intra-task correlation.

C.2. Measuring Substantive Fairness from the LLM-in-the-loop Evaluator

In what follows, we illustrate procedures on obtaining the **maxROR** (Equation (17)) for different treatments as a measurement of substantive fairness from our LLM-in-the-loop evaluator. The **maxROR** is obtained from the fitted GEE Equation (15), which provides model-based probabilities of correct prediction for each treatment and group.

First, define the notation of the estimated coefficients from fitting (15): let

- $\hat{\beta}_0$ be the estimated intercept
- $\hat{\beta}_t^{\text{treatment}}$ be the estimated coefficient for treatment t
- $\hat{\beta}_a^{\text{group}}$ be the estimated coefficient for group a
- $\hat{\beta}_{t:a}$ be the estimated coefficient for the interaction of treatment t and group a ,
- $\hat{\beta}_{\text{diff}}$ be the estimated coefficient for difficulty
- $\hat{\beta}_{\text{adopt}}$ be the estimated coefficient for adoption

In model (15), both treatment and group are categorical covariates, with control being the baseline category of treatment. Consider a non-control treatment t and a group a , we define the model-based marginal probability of a correct response for treatment t in group a as

$$p_{t,a} := \frac{1}{N_{t,a}} \sum_{j \in \mathcal{I}_{t,a}} \text{logit}^{-1} \left(\hat{\beta}_0 + \hat{\beta}_t^{\text{treatment}} + \hat{\beta}_a^{\text{group}} + \hat{\beta}_{t:a} + \hat{\beta}_{\text{diff}} \text{diff}_j + \hat{\beta}_{\text{adopt}} \text{adoption}_{j,t} \right), \quad (\text{A12})$$

where $\mathcal{I}_{t,a}$ is the set of predictions in group a that are applied treatment t , and $N_{t,a}$ is the cardinality of the set $\mathcal{I}_{t,a}$. Thus, the $p_{t,a}$ defined in (A12) is the model-based average probability that the LLM's prediction is correct, obtained by evaluating the fitted GEE at treatment t and group a while plugging in each task's difficulty and adoption rate under treatment t , and then averaging these predicted probabilities over all tasks in group a .

Similarly, for the baseline treatment “control” and group a , we define

$$\begin{aligned} p_{\text{control},a} &:= \frac{1}{N_{\text{Control},a}} \sum_{j \in \mathcal{I}_{\text{Control},a}} \text{logit}^{-1} \left(\hat{\beta}_0 + \hat{\beta}_{\text{Control}}^{\text{treatment}} + \hat{\beta}_a^{\text{group}} + \hat{\beta}_{\text{Control}:a} + \hat{\beta}_{\text{diff}} \text{diff}_j + \hat{\beta}_{\text{adopt}} \text{adoption}_{j,\text{Control}} \right) \\ &= \frac{1}{N_{\text{Control},a}} \sum_{j \in \mathcal{I}_{\text{Control},a}} \text{logit}^{-1} \left(\hat{\beta}_0 + \hat{\beta}_a^{\text{group}} + \hat{\beta}_{\text{diff}} \text{diff}_j \right), \end{aligned} \quad (\text{A13})$$

which is the model-based probability of a correct response under control in group a .

Then, for non-control treatment t and every protected group a , the OR of t versus control is given by

$$\text{OR}_{t,a} := \frac{p_{t,a}/(1-p_{t,a})}{p_{\text{control},a}/(1-p_{\text{control},a})}$$

For each protected group, the ORs assess how much more likely an LLM under treatment t is to give the correct response than if it were in the control. If $\text{OR}_{t,a} > 1$, then for group a the odds that the LLM produces a correct response under treatment t are higher than them under the control, and if $\text{OR}_{t,a} < 1$ they are lower.

The disparity of treatment effect on prediction accuracy is quantified by the ROR. For treatment t , the ROR between group a and group b is computed as

$$\text{ROR}_{t,a,b} := \frac{\text{OR}_{t,a}}{\text{OR}_{t,b}} - 1$$

If $\text{ROR}_{t,a,b} \approx 0$, treatment t provides the same treatment effect over the Control for group a as it does for group b , indicating fairness of treatment effect from t on prediction accuracy between the two groups. As mentioned in Section 4.2, to compare the parity of conformal methods' impact on prediction accuracy, we compute and compare the **maxROR**

$$\text{maxROR}_t := \max_{a,b \in \mathcal{A}} \text{ROR}_{t,a,b}$$

for each non-control treatment t . For any two treatments t_1 and t_2 , if $\mathbf{maxROR}_{t_1} > \mathbf{maxROR}_{t_2}$, then treatment t_1 induces a greater disparity in prediction accuracy across protected groups than treatment t_2 . In this case, compared to t_1 , treatment t_2 is preferred if the goal is to achieve fairness in downstream prediction accuracy under the assistance of prediction sets.

D. Additional Experiment Details

D.1. Dataset Details

We consider four prediction tasks with open-access fairness datasets where algorithmic assistance may benefit human decision making. Across all tasks, we construct prediction sets using conformal prediction methods applied to the outputs of task-specific base models.

Image Classification. Image classification is widely used in high-stakes applications, including medical screening and surveillance, where biases may lead to serious societal consequences. Prior fairness research in visual domains has investigated facial recognition systems (Buolamwini & Gebru, 2018), medical image analysis (Drukker et al., 2023), and methods for improving fairness in image classification models (Yang et al., 2024b). To model a similar scenario, we use the **Facet** dataset (Gustafson et al., 2023), which consists of images of people labeled by occupation and grouped by age. We retain the 20 most common occupation classes: [*Backpacker, Boatman, Computer User, Craftsman, Farmer, Guard, Guitarist, Gymnast, Hairdresser, Horse Rider, Laborer, Officer, Motorcyclist, Painter, Repairman, Salesperson, Singer, Skateboarder, Speaker, Tennis Player*], and split the data into calibration (\mathcal{D}_{cal}), calibration-validation ($\mathcal{D}_{\text{calval}}$), and test ($\mathcal{D}_{\text{test}}$) sets, stratified by class. Age annotations are provided in four predefined groups: *Younger, Middle, Older, and Unknown*; see Table 3 for group distributions in $\mathcal{D}_{\text{calval}}$, \mathcal{D}_{cal} and $\mathcal{D}_{\text{test}}$. We employ CLIP ViT-L/14 (Radford et al., 2021) as a zero-shot image classifier to generate class scores, to which conformal prediction is applied. **Facet** is distributed under Meta’s **Facet** usage agreement (custom license) and is intended for evaluation only; using **Facet** annotations for training is prohibited.

Text Classification. Text classification is commonly used to organize large volumes of text input, for example in hiring or recruitment, where demographic biases may arise. As a surrogate task, we use the **BiosBias** dataset (De-Arteaga et al., 2019), which contains personal biographies labeled by occupation and grouped by binary gender. We select the 10 most frequent occupations [*Professor, Physician, Photographer, Journalist, Psychologist, Teacher, Dentist, Surgeon, Painter, and Model*] and partition the dataset into $\mathcal{D}_{\text{train}}$, \mathcal{D}_{val} , \mathcal{D}_{cal} , $\mathcal{D}_{\text{calval}}$, and $\mathcal{D}_{\text{test}}$, ensuring class balance across splits. See Table 4 for binary group distributions in $\mathcal{D}_{\text{calval}}$, \mathcal{D}_{cal} and $\mathcal{D}_{\text{test}}$. A pre-trained BERT model (Devlin et al., 2019) is used to generate text representations, on which we train a linear classifier. Conformal prediction is applied using the classifier’s output scores. The code and data-generation pipeline for BiosBias is released under the MIT License.

Audio Emotion Recognition. Emotion recognition arises naturally in human communication, though emotional expression can vary across speakers from different demographic groups. We use the **RAVDESS** dataset (Livingstone & Russo, 2018), which contains audio recordings of professional actors expressing eight emotions [*Happy, Angry, Calm, Fearful, Neutral, Disgust, Sad and Surprised*] using identical short phrases, with speakers grouped by binary gender. The dataset is split into \mathcal{D}_{cal} , $\mathcal{D}_{\text{calval}}$, and $\mathcal{D}_{\text{test}}$, stratified by emotion class and gender (see Table 5). We adopt a fine-tuned wav2vec 2.0 model (Baevski et al., 2020; Grosman, 2021; Fadel, 2023) for emotion classification. **RAVDESS** is released under the Creative Commons Attribution-NonCommercial-ShareAlike 4.0 International license (CC BY-NC-SA 4.0).

Tabular Data Prediction. Tabular prediction tasks arise in many real-world decision-making settings, including banking, insurance underwriting, credit risk assessment, and public policy, where structured demographic and socioeconomic features are used to inform consequential decisions. We consider a tabular prediction setting using the **ACSIncome** dataset from the Folktables benchmark (Ding et al., 2021), which is derived from the 2023 U.S. Census data. Race is treated as the sensitive attribute for group-based evaluation. We re-grouped the race attribute to five categories [*White alone, Black or African American alone, Asian alone, Two or More Races, All Other Races (Aggregated)*]. The task is to predict the income level of an individual among 10 predefined income brackets [104 - 9000, 9000 - 20000, 20000 - 30000, 30000 - 38800, 38800 - 48450, 48450 - 60000, 60000 - 75000, 75000 - 96900, 96900 - 140000, 140000 - 1672000], using features such as education, employment, and household characteristics. We partition the dataset into calibration (\mathcal{D}_{cal}), calibration-validation ($\mathcal{D}_{\text{calval}}$), and test ($\mathcal{D}_{\text{test}}$) splits, with stratification by income bracket. Refer to Table 6 for group distributions in $\mathcal{D}_{\text{calval}}$, \mathcal{D}_{cal} and $\mathcal{D}_{\text{test}}$. For classification, we employ an XGBoost model (Chen & Guestrin, 2016), and apply conformal prediction to the model’s output scores. **ACSIncome** is derived from the U.S. Census Bureau’s American Community Survey (ACS) Public Use Microdata Sample (PUMS); use of the underlying ACS PUMS data is governed by the Census Bureau’s terms of service.

Table 3. FACET Group Counts.

GROUP	$\mathcal{D}_{\text{CALVAL}}$	\mathcal{D}_{CAL}	$\mathcal{D}_{\text{TEST}}$
YOUNGER	254	711	276
MIDDLE	772	2144	729
OLDER	103	299	91
UNKNOWN	271	846	304
TOTAL	1400	4000	1400

Table 4. BiosBias Group Counts.

GROUP	$\mathcal{D}_{\text{CALVAL}}$	\mathcal{D}_{CAL}	$\mathcal{D}_{\text{TEST}}$
FEMALE	2424	4887	969
MALE	2576	5113	1031
TOTAL	5000	10000	2000

Table 5. RAVDESS Group Counts.

GROUP	$\mathcal{D}_{\text{CALVAL}}$	\mathcal{D}_{CAL}	$\mathcal{D}_{\text{TEST}}$
FEMALE	120	420	180
MALE	120	420	180
TOTAL	240	840	360

Table 6. ACSIncome Group Counts.

GROUP	$\mathcal{D}_{\text{CALVAL}}$	\mathcal{D}_{CAL}	$\mathcal{D}_{\text{TEST}}$
WHITE	6655	13487	6637
BLACK OR AFRICAN AMERICAN	842	1560	819
ASIAN	662	1362	663
TWO OR MORE RACES	1134	2164	1117
ALL OTHER RACES	707	1427	764
TOTAL	10000	20000	10000

D.2. Score Functions Used for Conformal Prediction

The Marginal, Mondrian, Label-Clustered and Group-Clustered CP considered in this paper are implemented using one of two nonconformity score functions: **RAPS** (Angelopoulos et al., 2021) or **SAPS** (Huang et al., 2024). A nonconformity score $s : \mathcal{X} \times \mathcal{Y} \rightarrow \mathbb{R}$ assigns a scalar value $s(x, y)$ to each candidate label y for an input x , where smaller values indicate that y is more compatible with x under the base model. Different CP procedures in our experiments differ only in how these scores are calibrated (e.g., global vs. group-wise vs. cluster-wise calibration), but they all use the same underlying score definitions below.

Notation. Let $\mathcal{Y} = \{1, \dots, L\}$ be the label set. For an input x , let $f(x) \in \mathbb{R}^L$ denote the model logits and define temperature-scaled softmax probabilities

$$p_y(x) = \frac{\exp(f_y(x)/T)}{\sum_{y' \in \mathcal{Y}} \exp(f_{y'}(x)/T)}, \quad T > 0.$$

Let $\pi_x(1), \dots, \pi_x(L)$ be labels sorted so that $p_{\pi_x(1)}(x) \geq p_{\pi_x(2)}(x) \geq \dots \geq p_{\pi_x(L)}(x)$, and define the rank

$$o_x(y) := \min\{k : \pi_x(k) = y\}.$$

We also use an independent randomization variable $u \sim \text{Unif}[0, 1]$ for tie-breaking.

RAPS. RAPS (Regularized Adaptive Prediction Sets (Angelopoulos et al., 2021)) combines a randomized cumulative-mass term with an explicit penalty on lower-ranked labels. Define the cumulative probability mass strictly above y by

$$\rho_x(y) := \sum_{k=1}^{o_x(y)-1} p_{\pi_x(k)}(x).$$

Given hyperparameters $\lambda \geq 0$ and $k_{\text{reg}} \in \{1, \dots, L\}$, the RAPS nonconformity score is

$$s_{\text{RAPS}}(x, y) := \rho_x(y) + u p_y(x) + \lambda(o_x(y) - k_{\text{reg}})_+, \quad (a)_+ := \max\{a, 0\}.$$

SAPS. SAPS (Sorted Adaptive Prediction Sets (Huang et al., 2024)) is a rank-based score that retains the ordering information while reducing dependence on small tail probabilities. Let $p_{\max}(x) := \max_{y'} p_{y'}(x) = p_{\pi_x(1)}(x)$. With hyperparameter $\lambda \geq 0$, define

$$s_{\text{SAPS}}(x, y) := \begin{cases} u p_y(x), & \text{if } o_x(y) = 1, \\ p_{\max}(x) + \lambda(o_x(y) - 2 + u), & \text{if } o_x(y) \geq 2. \end{cases}$$

D.3. Hyperparameters

Tuning hyperparameters in RAPS and SAPS. To construct CP sets, we split the data into three disjoint parts: a tuning set $\mathcal{D}_{\text{calval}}$, a calibration set \mathcal{D}_{cal} , and a test set $\mathcal{D}_{\text{test}}$. Hyperparameters in the score functions are selected using $\mathcal{D}_{\text{calval}}$. After tuning, conformal thresholds are computed on \mathcal{D}_{cal} with the chosen hyperparameters. Prediction sets used in the LLM-in-the-loop evaluator for the downstream task are then obtained on $\mathcal{D}_{\text{test}}$.

We tune hyperparameters by using Bayesian optimization via the Optuna library (Akiba et al., 2019), coupled with the TPESampler for efficient search over 50 iterations to minimize average set size. For each set of candidate hyperparameters, we (i) compute the conformal threshold(s) \hat{q} from \mathcal{D}_{cal} , (ii) form prediction sets according to the rules of CP methods on $\mathcal{D}_{\text{calval}}$, and (iii) score the hyperparameters candidate by the average set size on $\mathcal{D}_{\text{calval}}$. We select the optimal hyperparameters as the minimizer of average set size. For Mondrian, Label-Clustered and Group-Clustered CP, the same set of hyperparameters is used across all groups/clusters during tuning, while the final conformal thresholds are calibrated separately within each group/cluster. Table 7 presents the final hyperparameters after the tuning procedure.

Table 7. Hyperparameter Settings for Each Dataset After Tuning

DATASET	SCORE FUNCTION	MARGINAL			MONDRIAN			LABEL-CLUSTERED			GROUP-CLUSTERED		
		T	λ	k_{reg}	T	λ	k_{reg}	T	λ	k_{reg}	T	λ	k_{reg}
FACET	RAPS	0.53	0.07	4	0.30	0.16	4	0.51	1.38	4	0.30	0.16	4
BIOSBIAS	SAPS	0.56	0.20	–	0.40	0.20	–	0.74	0.28	–	0.47	0.19	–
RAVDESS	RAPS	0.16	1.61	3	0.15	0.69	3	0.17	0.35	3	0.16	0.51	3
ACSIMCOME	RAPS	0.09	0.05	4	0.10	0.05	4	0.09	0.05	4	0.09	0.05	4

Hyperparameters in Clustered CP. As described in Appendix B, we use a proportion parameter γ to determine the size of the clustering subset, $\lfloor \gamma n_{\text{cal}} \rfloor$, which is used to learn the cluster assignments. In our experiments, we set $\gamma = 0.3$, which provides sufficient data to estimate stable cluster structure while leaving enough observations in the remaining calibration set to estimate conformal thresholds. Following Ding et al. (2023), we use $\{0.5, 0.6, 0.7, 0.8, 0.9\} \cup \{1 - \alpha\}$ -quantiles of a score distribution of class/group as the embedding vector for clustering.

To ensure these quantile features are well-defined, we set $n_{\alpha} = (1/\alpha) - 1$ (e.g., $n_{\alpha} = 9$ when $\alpha = 0.1$), the minimum sample size for which the empirical $(1 - \alpha)$ -quantile is finite. Any class/group with at most n_{α} observations in the clustering subset is assigned to a *null* cluster; the remaining classes/groups are embedded via the above quantiles and clustered using k -means.

Hyperparameters and implementation of Backward CP. In our implementation of Backward CP, we do not use RAPS or SAPS score functions, instead, we use the cross-entropy loss as the score to compute the e-value. Let $f(x) \in \mathbb{R}^{|\mathcal{Y}|}$ denote model logits and $p(y|x) = \text{softmax}(f(x))_y$. We use the cross-entropy loss

$$s_{\text{NLL}}(x, y) = -\log(p(y|x) + \epsilon),$$

with $\epsilon > 0$ for numeric stability so the score is well-defined even when $p(y|x) = 0$. In our experiment, we set $\epsilon = 1e-4$. Given calibration data $\{(X_i, Y_i)\}_{i=1}^n$, define $S_i = s_{\text{NLL}}(X_i, Y_i)$. For a test input x_{test} and candidate label y , compute the e-value

$$E_{\text{test}}(y) = \frac{(n+1)s_{\text{NLL}}(x_{\text{test}}, y)}{\sum_{i=1}^n S_i + s_{\text{NLL}}(x_{\text{test}}, y)}.$$

For any $\alpha \in (0, 1)$, the prediction set is

$$\mathcal{C}_n^{\alpha}(x_{\text{test}}) = \{y \in \mathcal{Y} : E_{\text{test}}(y) < 1/\alpha\},$$

using a strict inequality to break ties.

Backward CP selects a data-dependent level $\tilde{\alpha}(x_{\text{test}})$ to satisfy a maximum set size constraint \mathcal{T} . In our implementation, the target size is

$$\mathcal{T} = \lceil \text{average set size from Marginal CP} \rceil + \text{offset}.$$

We choose $\tilde{\alpha}$ as the smallest $\alpha \in [\epsilon', 1 - \epsilon']$ (set $\epsilon' = 1e-4$) such that $|\mathcal{C}_n^{\alpha}| \leq \mathcal{T}$. The $\tilde{\alpha}$ is computed by binary search up to a tolerance parameter (which we set to $1e-7$). If the resulting set is empty, we increase \mathcal{T} by one and repeat to ensure a

nonempty prediction set. Moreover, the offset starts from 0, and we increase it iteratively until the empirical coverage meets the target $1 - \alpha$ up to a fixed maximum number of iterations, which we set to be 10.

D.4. Prompts Used for LLM-in-the-loop Evaluator

For LLM-based downstream prediction tasks, we use different LLMs depending on the modality and dataset: Qwen2.5-VL-7B-Instruct (<https://huggingface.co/Qwen/Qwen2.5-VL-7B-Instruct>) for FACET (vision-language), GPT-4o-mini (<https://platform.openai.com/docs/models/gpt-4o-mini>) and Llama-3.2-3B (<https://huggingface.co/meta-llama/Llama-3.2-3B>) for BiosBias (text), GPT-4o-audio-preview (<https://platform.openai.com/docs/models/gpt-4o-audio-preview>) for RAVDESS (audio), and Qwen2.5-7B (<https://huggingface.co/Qwen/Qwen2.5-7B>) for ACSIncome (tabular and text-only prompting). These choice reflect modality compatibility and were held fixed across CP methods within each dataset to ensure fair comparisons.

The prompt templates used in our experiments are as follows:

1. FACET

You are given an image of a person and a list of possible classes: [{all_options}]. Select exactly one class name from this list. Respond with only the class name. Do not provide explanations or additional text.

image attached
The following shorter list contains classes that are more likely to be correct:
[{options}]
Based on the image, which class is the person most likely to belong to?

Control:

You are given an image of a person and a list of possible classes: [{all_options}]. Select exactly one class name from this list. Respond with only the class name. Do not provide explanations or additional text.

image attached
Based on the image, which class is the person most likely to belong to?

2. BiosBias

You are an HR expert. Given a short biography, select the correct occupation from the provided list: [{all_options}]. Respond with only the occupation name from this list. Do not explain your reasoning.

Biography:
{prompt}
The following shorter list contains occupations that are more likely to be correct:
[{options}]
Based on the biography above, which occupation is the best match?

Control:

You are an HR expert. Given a short biography, select the correct occupation from the provided list: [{all_options}]. Respond with only the occupation name from this list. Do not explain your reasoning.

Biography:
{prompt}
Based on the biography above, which occupation is the best match?

3. RAVDESS

You are an expert in emotion classification from audio.

Instructions:

- Focus on HOW they speak, not WHAT they say
- Listen for vocal tone, pitch patterns, and energy
- Classify which emotion does the audio convey

Choose one emotion from this list: {{all_options}}

Answer with ONE word from the list only.

Prediction set from a classifier with {coverage_info} confidence to contain the true answer: {{options}}

Listen carefully to the speaker's voice. Analyze:

1. Vocal tone
2. Pitch patterns (high/low, rising/falling)
3. Speaking energy
4. Emotional expression in delivery

Based on these cues in the audio, which emotion best matches the speaker's vocal expression?

Control:

You are an expert in emotion classification from audio.

Instructions:

- Focus on HOW they speak, not WHAT they say
- Listen for vocal tone, pitch patterns, and energy
- Classify which emotion does the audio convey

Choose one emotion from this list: {{all_options}}

Answer with ONE word from the list only.

Listen carefully to the speaker's voice. Analyze:

1. Vocal tone
2. Pitch patterns (high/low, rising/falling)
3. Speaking energy
4. Emotional expression in delivery

Based on these cues in the audio, which emotion best matches the speaker's vocal expression?

Choose from: {{all_options}}

4. ACSIncome

You are a labor economics expert. Given a structured demographic and employment profile from a census survey, select the correct income bracket from the provided list: {{all_options}}.

Respond with only the income bracket label. Do not explain your reasoning.

Profile: The following is a structured demographic and employment profile derived from a census survey.

Age: {AGEP}

Class of worker: {COW}

Educational attainment: {SCHL}

Marital status: {MAR}

Occupation code: {OCCP}

Place of birth: {POBP}

Employment status of parent: {ESP}

Relationship to household reference person: {RELSHIPP}

Usual hours worked per week (past 12 months): {WKHP}

Sex: {SEX}

Race: {RAC1P}

The following income brackets are more likely to be correct: {{options}}

Based on the profile above, which income bracket is the best match?

Control:

You are a labor economics expert. Given a structured demographic and employment profile from a census survey, select the correct income bracket from the provided list:
[*{all_options}*]).

Respond with only the income bracket label. Do not explain your reasoning.

Profile: The following is a structured demographic and employment profile derived from a census survey.

Age: {AGEP}

Class of worker: {COW}

Educational attainment: {SCHL}

Marital status: {MAR}

Occupation code: {OCCP}

Place of birth: {POBP}

Employment status of parent: {ESP}

Relationship to household reference person: {RELSHIPP}

Usual hours worked per week (past 12 months): {WKHP}

Sex: {SEX}

Race: {RAC1P}

Based on the profile above, which income bracket is the best match?

E. Details and Results from the LLM-in-the-loop Evaluator

E.1. Comparing Human-in-the-loop and LLM-in-the-loop Evaluators

We present a detailed comparison between our LLM-in-the-loop evaluator and the prior human-in-the-loop evaluator (Cresswell et al., 2025) to show the validity of using the LLM-in-the-loop evaluator as a scalable proxy for assessing substantive fairness of CP methods. Moreover, we use our experimental results to illustrate how we calibrate the LLM-in-the-loop evaluator so that it captures the key behaviors of substantive fairness discovered in the prior study with human subjects.

Adoption-rate-difference in human vs. LLM. The following Table 8, Table 9, and Table 10 present the adoption rate (proportion of predicted labels contained in the provided prediction set) of the prior human subjects and the LLMs used in our experiments. Here, we consider the intersection of the CP methods (Marginal and Mondrian) and datasets (FACET, BiosBias, RAVDESS) between the ones used by Cresswell et al. (2025) and in our experiments. As observed from the tables, overall, LLMs have higher adoption rates compared to human subjects, indicating that LLMs tend to closely follow the prompt and rely on the provided prediction set when making decisions. In nearly experiments, we found that this tendency of high reliance on provided sets is more prominent when using more capable LLMs.

Calibrate the LLM-in-the-loop evaluator. As LLMs are more dependent on the provided prediction set when outputting a response, accuracy differs systematically across adoption status, and invalid responses (answers that are outside of the label space) often occur when the LLM does not pick a label from the provided set (see Table 11). Given that adoption is strongly predictive of downstream correctness from LLM, we treat adoption as an outcome-relevant covariate so that estimated treatment effects compare methods at comparable levels of reliance on the prediction set.

Here, we include an example of **maxROR** computed from the GEE without the adoption covariate to illustrate that omitting adoption can yield misleading conclusions on substantive fairness, because treatments and groups may be compared at different (and uneven) levels of reliance on the provided set. As what described in Section 4.2, for each test x_j in BiosBias and treatment t , we ask LLM to predict y_j based on $x_j, \mathcal{C}_t(x_j)$, and the stated coverage guarantee M times (in the control case, no prediction set is provided). Then, we compute the R_{jt} , which is the proportion of correct responses for x_j under treatment t out of the M predictions, and fit to the GEE proposed by Cresswell et al. (2025):

$$\text{logit}(\mathbb{E}[R_{jt}]) \sim \text{treatment}_t \times \text{group}_j + \text{diff} \quad (\text{A14})$$

The **OR** and **maxROR** are computed based on the fitted Equation (A14) according to the same logic described in Appendix C.2. The results are shown in Table 12. As we can see, in this case, $\text{maxROR}_{\text{Marginal}} > \text{maxROR}_{\text{Mondrian}}$, which does not align with the behavior discovered by Cresswell et al. (2025). This is because the LLM’s adoption rate for the Male group under the Marginal treatment is extremely high (98.20%; see Table 9). As a result, predictions for the Male group benefit disproportionately from the Marginal treatment, inflating $\text{OR}_{\text{Marginal, Male}}$ and hence $\text{maxROR}_{\text{Marginal}}$. This counterexample motivates including “adoption” as a covariate in the GEE.

Alignment with human-in-the-loop experiments. To make our evaluator reflect the substantive-fairness pattern discovered by Cresswell et al. (2025) while respecting the different experimental design, we treat each task instance as the clustering unit in the GEE Equation (15) with adoption as a covariate. From the results shown in Appendix E.2 (also summarized in Table 2), we see that the LLM-in-the-loop evaluator outputs $\text{maxROR}_{\text{Marginal}} < \text{maxROR}_{\text{Mondrian}}$ in our experiments on FACET, BiosBias, and RAVDESS. Moreover, the **maxROR** shows a pattern that it is small when the set size disparity between sensitive groups is small (e.g., in the case of Marginal, Label-Clustered, or Backward), and the **maxROR** is large for Mondrian and Group-Clustered CP, which have large set size disparity due to equalizing coverage across groups. This trend of **maxROR** reflects the downstream prediction behavior discovered by Cresswell et al. (2025), validating that the LLM-in-the-loop evaluator captures key properties of substantive fairness revealed in the prior human-in-the-loop study, and supporting the use of the LLM-in-the-loop evaluator as a proxy for assessing substantive fairness across CP methods.

Table 8. Adoption rate of human vs. LLM (Qwen2.5-VL-7B-Instruct) for FACET

TREATMENT	GROUP	HUMAN ADOPTION%	LLM ADOPTION%
MARGINAL	MIDDLE	92.82	96.52
	OLDER	91.66	90.66
	UNKNOWN	96.76	99.01
	YOUNGER	94.79	98.23
MONDRIAN	MIDDLE	93.22	96.42
	OLDER	92.91	92.17
	UNKNOWN	96.76	98.68
	YOUNGER	96.66	98.05

Table 9. Adoption rate of human vs. LLM (GPT-4o-mini) for BiosBias

TREATMENT	GROUP	HUMAN ADOPTION%	LLM ADOPTION%
MARGINAL	FEMALE	92.31	95.22
	MALE	93.87	98.20
MONDRIAN	FEMALE	92.30	92.07
	MALE	94.48	97.36

Table 10. Adoption rate of human vs. LLM (GPT-4o-audio-preview) for RAVDESS

TREATMENT	GROUP	HUMAN ADOPTION%	LLM ADOPTION%
MARGINAL	FEMALE	90.67	91.89
	MALE	87.97	92.44
MONDRIAN	FEMALE	91.95	90.00
	MALE	92.20	94.11

 Table 11. Empirical probabilities of correct response and invalid response conditioning on adoption status for FACET, BiosBias, and RAVDESS datasets. As we can see, the $\mathbb{P}(\text{correct} | \text{adoption} = 1)$ is higher than $\mathbb{P}(\text{correct} | \text{adoption} = 0)$, especially for the challenging FACET and RAVDESS tasks.

	FACET	BIOSBIAS	RAVDESS
$\mathbb{P}(\text{CORRECT} \text{ADOPTION} = 1)$	78.40%	80.64%	46.58%
$\mathbb{P}(\text{CORRECT} \text{ADOPTION} = 0)$	37.99%	76.74%	0.00%
$\mathbb{P}(\text{INVALID} \text{ADOPTION} = 0)$	25.14%	9.30%	41.75%

 Table 12. The **OR** and **maxROR** computed from fitting a GEE without the “adoption” covariate for BiosBias. As shown on the table, $\mathbf{OR}_{\text{Marginal, Male}}$ has a relatively large value from the relatively high adoption rate, resulting in larger $\mathbf{maxROR}_{\text{Marginal}}$ than $\mathbf{maxROR}_{\text{Mondrian}}$.

GROUP	$\mathbf{OR}_{\text{MARGINAL}}$	$\mathbf{OR}_{\text{MONDRIAN}}$	$\mathbf{MAXROR}_{\text{MARGINAL}}(\%)$	$\mathbf{MAXROR}_{\text{MONDRIAN}}(\%)$
FEMALE	1.026	1.219		
MALE	1.308	1.110	27.4	9.9

E.2. LLM-in-the-loop Evaluator Results on Different Tasks

In Table 13 through Table 17 we show more detailed statistics from LLM-in-the-loop experiments of Section 6.2 across datasets and CP methods. In particular, we provide one ablation on BiosBias where our standard LLM GPT-4o-mini was replaced with Llama-3.2-3B (Grattafiori et al., 2024), demonstrating that qualitatively similar results can be obtained from distinct LLMs on the same task.

Table 13. Accuracy and fairness result on BiosBias experiment with *GPT-4o-mini* as the LLM-in-the-loop.

TREATMENT	CVG (GAP)%	SIZE (GAP)	ACCURACY (GAP)%	MAXROR%
CONTROL			78.96 (2.86)	
MARGINAL	89.5 (2.75)	1.68 (.050)	80.71 (3.75)	6.9
MONDRIAN	90.0 (.220)	1.80 (.474)	80.96 (3.90)	8.1
LABEL-CLUSTERED	90.2 (2.80)	1.81 (.033)	79.72 (2.55)	1.6
GROUP-CLUSTERED	90.2 (.193)	1.75 (.419)	81.05 (4.53)	12.5
BACKWARD	91.5 (1.87)	2.50 (.025)	79.41 (2.87)	0.3

 Table 14. Accuracy and fairness result on BiosBias experiment with *Llama-3.2-3B* as the LLM-in-the-loop.

TREATMENT	CVG (GAP)%	SIZE (GAP)	ACCURACY (GAP)%	MAXROR%
CONTROL			67.54 (4.97)	
MARGINAL	89.7 (2.76)	1.69 (.027)	76.03 (3.28)	50.0
MONDRIAN	89.1 (0.00)	1.70 (.435)	75.98 (5.03)	66.3
LABEL-CLUSTERED	90.1 (.019)	1.78 (.067)	74.83 (1.55)	36.0
GROUP-CLUSTERED	90.3 (.010)	1.74 (.343)	75.74 (4.30)	59.3
BACKWARD	91.5 (.018)	2.49 (.016)	71.19 (1.38)	36.2

 Table 15. Accuracy and fairness result on RAVDESS experiment with *GPT-4o-audio-preview* as the LLM-in-the-loop.

TREATMENT	CVG (GAP)%	SIZE (GAP)	ACCURACY (GAP)%	MAXROR%
CONTROL			21.11 (0.67)	
MARGINAL	88.33 (5.56)	1.89 (.039)	44.28 (1.00)	10.5
MONDRIAN	87.50 (.556)	1.86 (.578)	44.56 (12.0)	79.2
LABEL-CLUSTERED	87.78 (2.22)	1.92 (.011)	46.22 (1.33)	12.1
GROUP-CLUSTERED	87.50 (.556)	1.90 (.594)	42.94 (15.44)	110.3
BACKWARD	91.94 (8.33)	2.48 (.011)	39.22 (2.22)	17.0

 Table 16. Accuracy and fairness result on FACET experiment with *Qwen2.5-VL-7B-Instruct* as the LLM-in-the-loop.

TREATMENT	CVG (GAP)%	SIZE (GAP)	ACCURACY (GAP)%	MAXROR%
CONTROL			74.04 (18.00)	
MARGINAL	89.9 (10.7)	2.62 (.738)	76.91 (16.27)	9.0
MONDRIAN	89.9 (3.02)	2.69 (2.68)	77.06 (21.71)	37.7
LABEL-CLUSTERED	89.1 (7.46)	2.92 (.356)	78.81 (14.47)	13.5
GROUP-CLUSTERED	89.1 (8.14)	2.50 (1.28)	77.22 (18.05)	14.5
BACKWARD	90.3 (8.85)	3.50 (.053)	75.54 (18.39)	8.5

 Table 17. Accuracy and fairness result on ACSIncome experiment with *Qwen2.5-7B* as the LLM-in-the-loop.

TREATMENT	CVG (GAP)%	SIZE (GAP)	ACCURACY (GAP)%	MAXROR%
CONTROL			14.70 (2.22)	
MARGINAL	89.8 (3.18)	5.35 (.256)	20.41 (3.15)	19.4
MONDRIAN	89.5 (3.87)	7.16 (1.08)	14.91 (1.59)	17.5
LABEL-CLUSTERED	89.9 (3.67)	5.33 (.270)	18.68 (2.88)	7.2
GROUP-CLUSTERED	89.8 (2.88)	5.37 (.410)	19.02 (5.05)	23.1
BACKWARD	92.3 (3.03)	6.50 (.010)	15.02 (4.37)	19.7

E.3. Bootstrap Results

To provide uncertainty estimates on the **maxROR** metric, we performed bootstrap sampling over the LLM’s task predictions, with results shown in Table 18 through Table 21.

Table 18. Mean accuracy (gap) and mean \pm one standard error for maxROR over 1,000 resamples for BiosBias experiment on Table 13

TREATMENT	ACCURACY (GAP)%	MAXROR%
CONTROL	79.01 (2.84)	
MARGINAL	80.79 (3.69)	$9.0 \pm .22$
MONDRIAN	81.06 (3.87)	$9.7 \pm .22$
LABEL-CLUSTERED	79.78 (2.54)	6.1 $\pm .16$
GROUP-CLUSTERED	81.15 (4.49)	$13.1 \pm .26$
BACKWARD	79.49 (2.82)	6.5 $\pm .16$

 Table 19. Mean accuracy (gap) and mean \pm one standard error for maxROR over 1,000 resamples for RAVDESS experiment on Table 15

TREATMENT	ACCURACY (GAP)%	MAXROR%
CONTROL	21.07 (.840)	
MARGINAL	44.26 (.820)	24.6 ± 1.1
MONDRIAN	44.56 (11.79)	70.0 ± 1.2
LABEL-CLUSTERED	46.09 (1.29)	23.4 $\pm .78$
GROUP-CLUSTERED	42.89 (15.25)	92.5 ± 1.5
BACKWARD	39.28 (2.17)	18.4 $\pm .49$

 Table 20. Mean accuracy (gap) and mean \pm one standard error for maxROR over 1,000 resamples for FACET experiment on Table 16

TREATMENT	ACCURACY (GAP)%	MAXROR%
CONTROL	73.64 (18.17)	
MARGINAL	76.69 (16.33)	23.4 $\pm .38$
MONDRIAN	76.26 (21.76)	$42.3 \pm .60$
LABEL-CLUSTERED	78.86 (14.64)	$28.5 \pm .44$
GROUP-CLUSTERED	77.04 (18.07)	$30.8 \pm .47$
BACKWARD	75.07 (18.43)	21.6 $\pm .35$

 Table 21. Mean accuracy (gap) and mean \pm one standard error for maxROR over 1,000 resamples for ACSIncome experiment on Table 17

TREATMENT	ACCURACY (GAP)%	MAXROR%
CONTROL	14.55 (2.27)	
MARGINAL	20.29 (3.22)	$32.6 \pm .45$
MONDRIAN	14.67 (1.55)	$30.9 \pm .45$
LABEL-CLUSTERED	18.38 (2.90)	23.4 $\pm .34$
GROUP-CLUSTERED	18.19 (5.06)	$32.2 \pm .43$
BACKWARD	15.10 (4.35)	$33.2 \pm .45$

F. Additional Tables and Plots

F.1. CP and LLM-in-the-loop Metrics by Group

For further insights, in this section we provide additional tables and plots that break down our experimental data showing statistics conditional on group variables.

Table 22. Continuation of Table 13. Results on BiosBias experiment for each group.

TREATMENT	GROUP	CVG%	SIZE	SINGLETON%	ACCURACY%
CONTROL	FEMALE				80.43
	MALE				77.58
MARGINAL	FEMALE	90.92	1.65	62.33	82.64
	MALE	88.17	1.70	60.14	78.89
MONDRIAN	FEMALE	89.89	1.56	65.33	82.97
	MALE	90.11	2.03	29.00	79.07
LABEL-CLUSTERED (K = 3)	FEMALE	91.64	1.79	44.58	81.03
	MALE	88.85	1.82	43.16	78.49
GROUP-CLUSTERED (K = 2)	FEMALE	90.30	1.53	69.66	83.38
	MALE	90.11	1.95	40.93	78.86
BACKWARD	FEMALE	92.47	2.49	0.00	80.89
	MALE	90.59	2.51	0.00	78.02

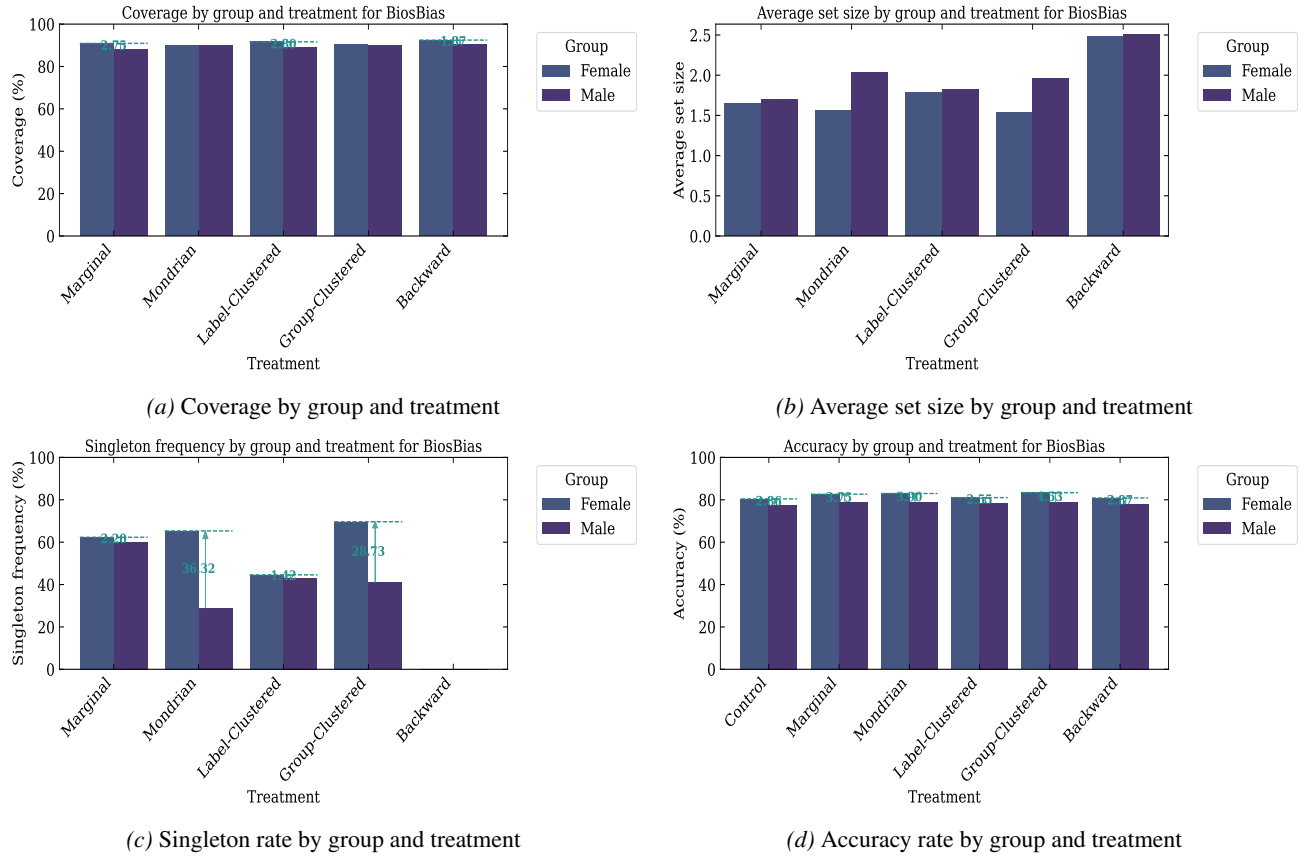


Figure 8. Experiment results of BiosBias with $K = 3$ in label-clustered CP and $K = 2$ in group-clustered CP. LLM-in-the-loop: GPT-4o-mini.

Table 23. Continuation of Table 15. Results on RAVDESS experiment for each group.

TREATMENT	GROUP	CVG%	SIZE	SINGLETON%	ACCURACY%
CONTROL	FEMALE				20.78
	MALE				21.44
MARGINAL	FEMALE	91.11	1.91	37.78	44.78
	MALE	85.56	1.87	40.56	43.78
MONDRIAN	FEMALE	87.78	1.57	57.78	50.56
	MALE	87.22	2.15	22.22	38.56
LABEL-CLUSTERED (K = 2)	FEMALE	88.89	1.92	30.56	46.89
	MALE	86.67	1.93	32.22	45.56
GROUP-CLUSTERED (K = 2)	FEMALE	87.22	1.61	56.11	50.67
	MALE	87.78	2.20	20.00	35.22
BACKWARD	FEMALE	96.11	2.47	0.00	40.33
	MALE	87.78	2.48	0.00	38.11

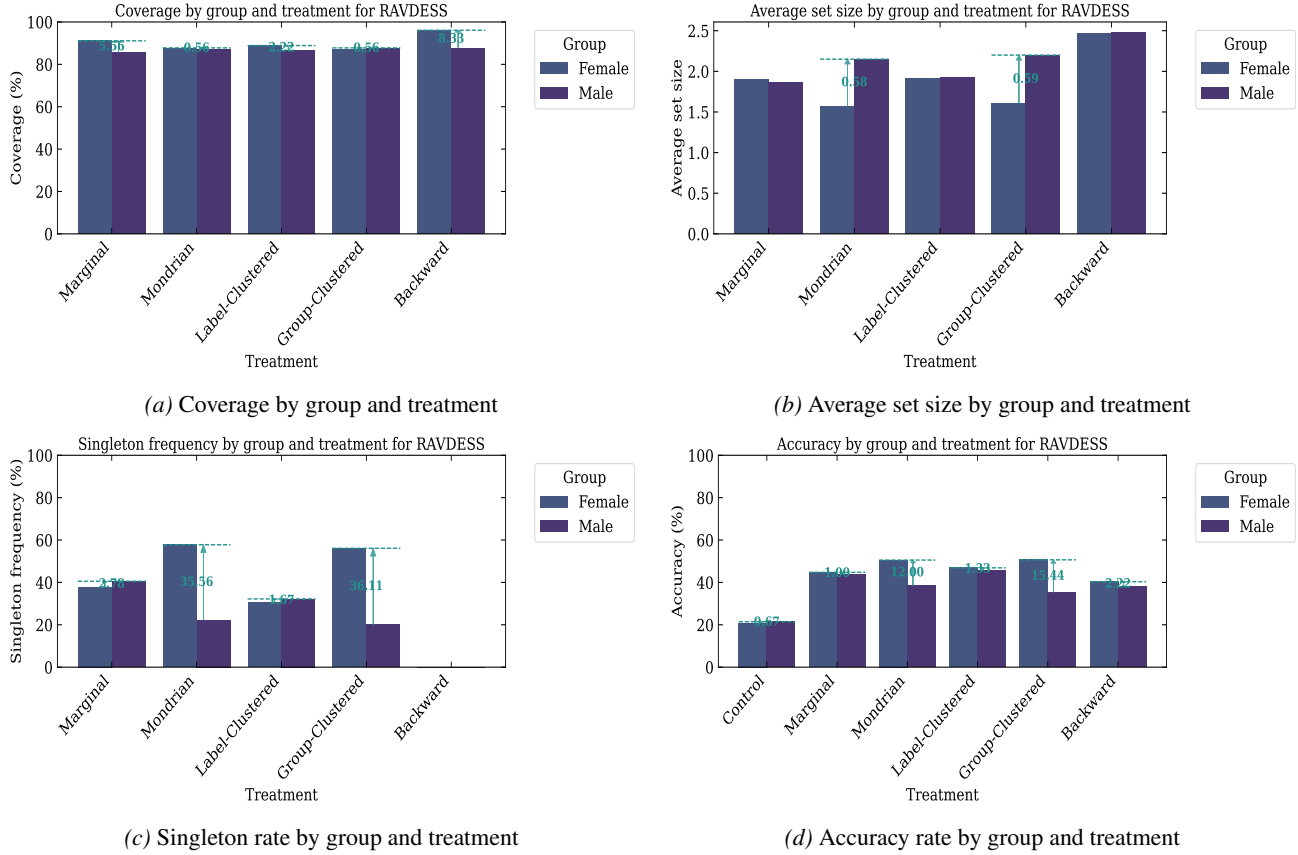

 Figure 9. Experiment results of RAVDESS with $K = 2$ in both label-clustered and group-clustered CP. LLM-in-the-loop: GPT-4o-audio-preview.

Table 24. Continuation of Table 16. Result on FACET experiment for each group.

TREATMENT	GROUP	CVG%	SIZE	SINGLETON%	ACCURACY%
CONTROL	MIDDLE				71.40
	OLDER				65.25
	UNKNOWN				74.63
	YOUNGER				83.24
MARGINAL	MIDDLE	88.61	2.72	29.22	74.49
	OLDER	84.62	2.91	18.68	69.51
	UNKNOWN	89.47	2.72	28.95	76.89
	YOUNGER	95.29	2.17	50.36	85.78
MONDRIAN	MIDDLE	89.16	2.93	24.14	74.21
	OLDER	89.01	4.31	0.00	65.38
	UNKNOWN	89.80	2.60	30.26	78.29
	YOUNGER	92.03	1.62	67.39	87.09
LABEL-CLUSTERED (K = 2)	MIDDLE	87.11	2.91	11.11	76.37
	OLDER	90.11	3.12	5.49	72.94
	UNKNOWN	88.49	3.00	8.88	78.62
	YOUNGER	94.57	2.76	9.78	87.41
GROUP-CLUSTERED (K = 2)	MIDDLE	89.03	2.87	25.10	74.02
	OLDER	84.62	3.04	15.38	68.41
	UNKNOWN	87.50	2.11	44.41	79.15
	YOUNGER	92.75	1.76	63.04	86.46
BACKWARD	MIDDLE	88.75	3.51	0.00	72.81
	OLDER	85.71	3.53	0.00	66.07
	UNKNOWN	91.45	3.49	0.00	76.81
	YOUNGER	94.57	3.47	0.00	84.47

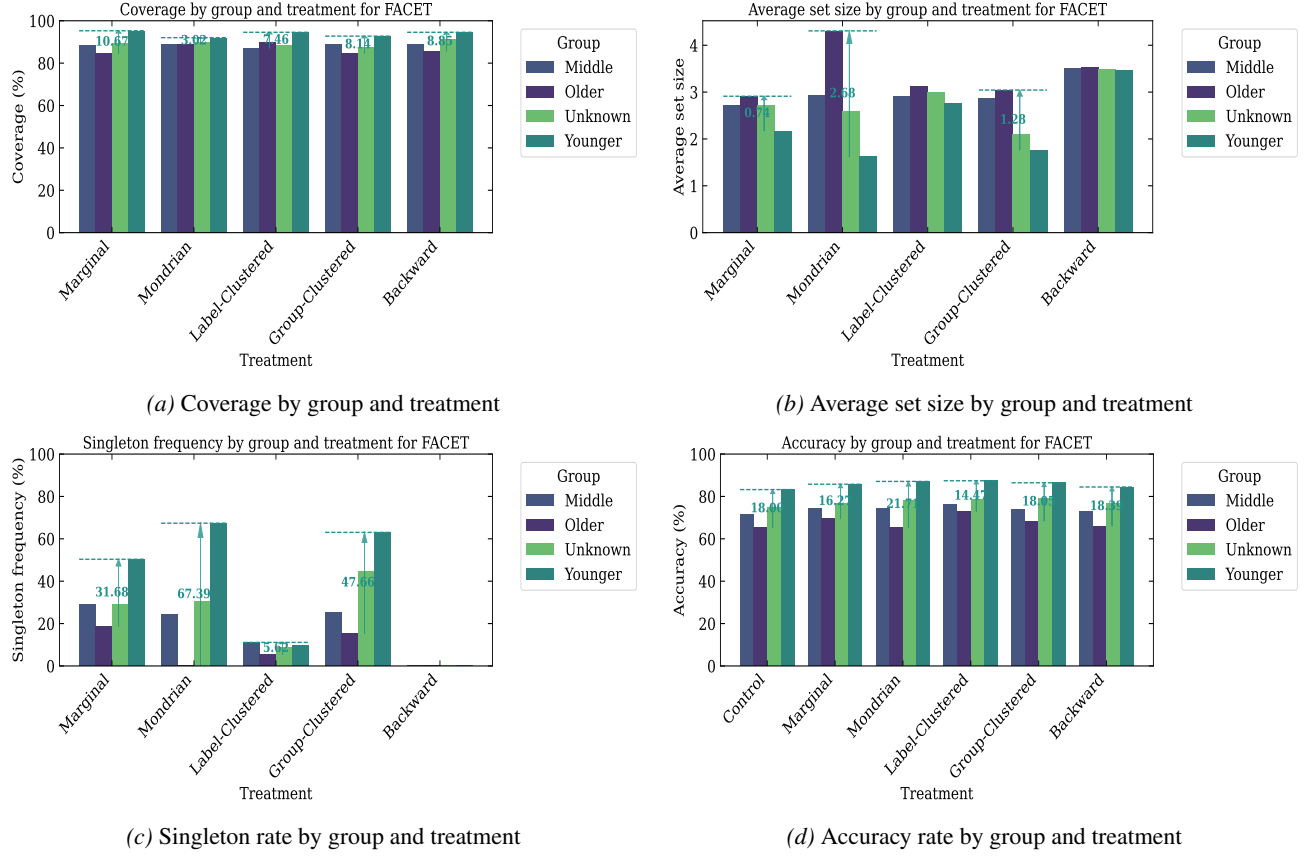


Figure 10. Experiment results of FACET with $K = 2$ in both label-clustered and group-clustered CP. LLM-in-the-loop: Qwen2.5-VL-7B-Instruct.

Table 25. Continuation of Table 17. Result on ACSIncome experiment for each group.

TREATMENT	GROUP	CVG%	SIZE	SINGLETON%	ACCURACY%
CONTROL	ALL OTHER RACES				15.12
	ASIAN				12.90
	BLACK OR AFRICAN AMERICAN				15.08
	TWO OR MORE RACES				15.02
	WHITE				14.72
MARGINAL	ALL OTHER RACES	87.83	5.44	.654	19.08
	ASIAN	87.33	5.19	2.71	18.74
	BLACK OR AFRICAN AMERICAN	88.77	5.34	2.44	21.89
	TWO OR MORE RACES	89.35	5.33	2.78	21.44
	WHITE	90.51	5.37	1.87	20.37
MONDRIAN	ALL OTHER RACES	90.58	7.98	0.00	15.58
	ASIAN	87.18	6.90	0.00	13.90
	BLACK OR AFRICAN AMERICAN	90.11	7.67	0.00	14.50
	TWO OR MORE RACES	91.05	7.64	0.00	14.19
	WHITE	89.33	6.95	.015	15.10
LABEL-CLUSTERED (K = 2)	ALL OTHER RACES	87.70	5.43	0.00	18.36
	ASIAN	87.03	5.16	0.00	16.48
	BLACK OR AFRICAN AMERICAN	88.52	5.32	0.00	19.35
	TWO OR MORE RACES	88.99	5.35	0.00	18.96
	WHITE	90.70	5.34	0.00	18.80
GROUP-CLUSTERED (K = 2)	ALL OTHER RACES	87.57	5.38	.262	18.55
	ASIAN	89.29	5.74	0.00	14.40
	BLACK OR AFRICAN AMERICAN	88.40	5.35	.366	19.29
	TWO OR MORE RACES	88.81	5.35	.537	19.32
	WHITE	90.45	5.33	.362	19.46
BACKWARD	ALL OTHER RACES	90.97	6.49	0.00	16.59
	ASIAN	89.89	6.49	0.00	12.25
	BLACK OR AFRICAN AMERICAN	90.84	6.49	0.00	15.23
	TWO OR MORE RACES	92.93	6.50	0.00	16.63
	WHITE	92.75	6.50	0.00	14.82

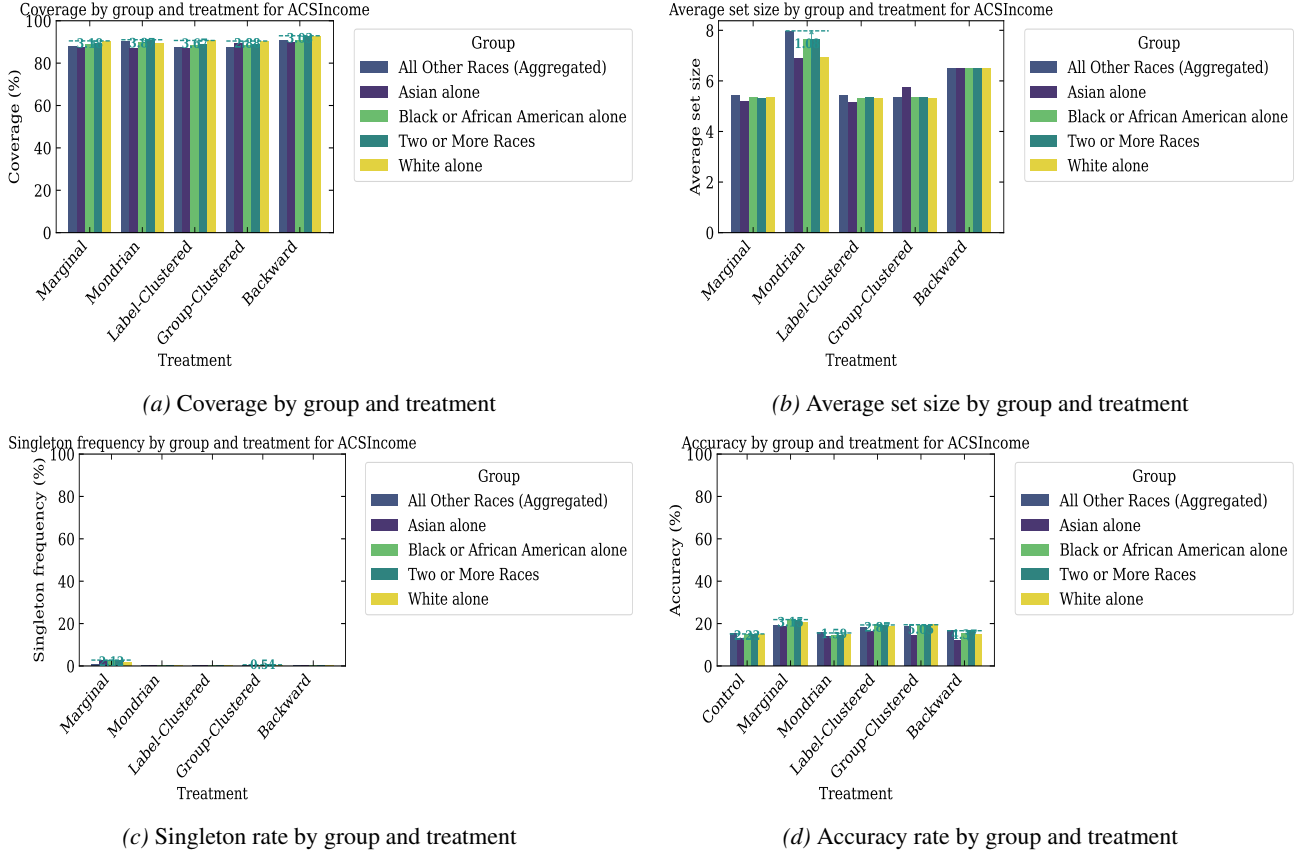


Figure 11. Experiment results of ACSIncome with $K = 2$ in both label-clustered and group-clustered CP. LLM-in-the-loop: Qwen2.5-7B.

F.2. Additional Coverage Gap and Set Size Gap Plots

In Section 6.3 we examined the coverage gap and set size gap across CP methods and two datasets. Figure 12 shows all four datasets together.

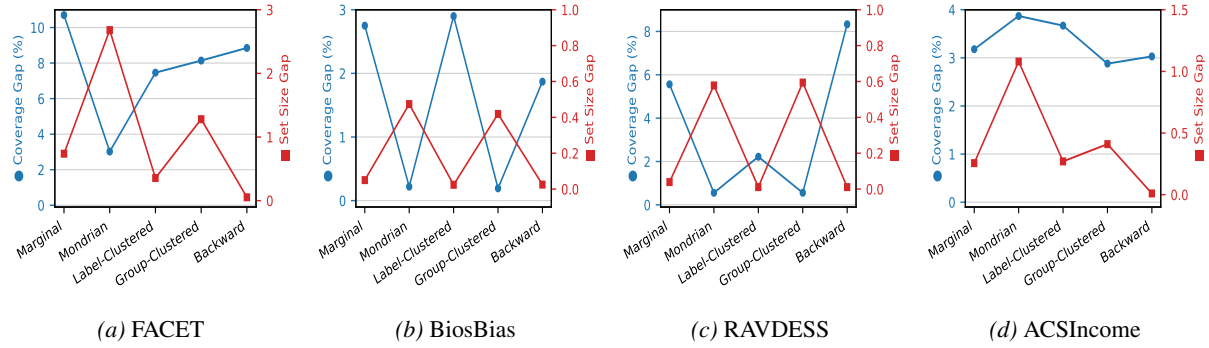


Figure 12. Coverage gap (blue dots, left axis) and set size gap (red squares, right axis) across CP methods on FACET, BiosBias, RAVDESS, and ACSIncome.